Vol. 483: 47–66, 2013
doi: 10.3354/meps10279

MARINE ECOLOGY PROGRESS SERIES
Mar Ecol Prog Ser

Published May 30

Inorganic C utilization and C isotope fractionation by pelagic and sea ice algal assemblages along the Antarctic continental shelf

Philippe D. Tortell[1,2,*], Mathew M. Mills[3], Christopher D. Payne[1], Maria T. Maldonado[1], Melissa Chierici[4,6], Agneta Fransson[5,7], Anne-Carlijn Alderkamp[3], Kevin R. Arrigo[3]

[1]Department of Earth, Ocean and Atmospheric Sciences, and [2]Department of Botany, University of British Columbia, Vancouver, British Columbia V6T 1Z4, Canada

[3]Department of Environmental Earth Systems Sciences, Stanford University, Stanford, California 94305, USA

[4]Department of Chemistry and Molecular Biology, University of Gothenburg, Göteborg 412 96, Sweden

[5]Department of Earth Sciences, University of Gothenburg, Box 460, 405 30 Göteborg, Sweden

[6]*Present address:* Institute of Marine Research, Postboks 6404, Tromsø 9294, Norway
[7]*Present address:* Norwegian Polar Institute, Fram Centre, Tromsø 9296, Norway

ABSTRACT: Physiological characteristics of inorganic C uptake were examined in Southern Ocean ice algae and phytoplankton assemblages. Ice algal and phytoplankton assemblages were largely dominated by diatoms and *Phaeocystis antarctica*, and showed a high capacity for HCO_3^- utilization, with direct HCO_3^- transport accounting for ~60% of total inorganic C uptake. Extracellular carbonic anhydrase (eCA) was detectable in all samples, but with significantly lower activity in sea ice algae. Neither HCO_3^- transport nor eCA activity was related to the *in situ* partial pressure of CO_2 (pCO_2) or taxonomic composition of samples. The half-saturation constant (K_S) for inorganic C ranged from ~100 to 5000 µM, and showed significantly more variability among sea ice algae than phytoplankton assemblages. For the phytoplankton assemblages, there were significant positive correlations between *in situ* pCO_2 and K_S (higher C substrate affinity in low pCO_2 waters), and also between K_S and maximum C uptake rates (V_{max}). In contrast, K_S and V_{max} in sea-ice algal assemblages were not correlated to each other, or to any other measured variables. The C isotope composition of particulate organic carbon (δ^{13}C-POC) in the phytoplankton assemblages showed modest variability (range –30 to –24.6‰) and was significantly correlated to the ratio of inferred growth rates (derived from V_{max}) and *in situ* CO_2 concentrations, but not to any measured C uptake parameters. δ^{13}C-POC in sea ice algal samples (range –25.7 to –12.9‰) was significantly heavier than in the phytoplankton assemblages, and not correlated to any other variables. Our results provide evidence for the widespread occurrence of carbon-concentrating mechanisms in Southern Ocean sea ice algae and phytoplankton assemblages.

KEY WORDS: Phytoplankton · Sea ice algae · Inorganic carbon uptake · HCO_3^- · Carbonic anhydrase

INTRODUCTION

Coastal waters surrounding the Antarctic continental shelf are regions of intense biological productivity (Smith & Nelson 1985, Arrigo et al. 1998, Arrigo & van Dijken 2003). Seasonal ice retreat leads to the formation of open water polynyas (Arrigo & van Dijken 2003), where large blooms of diatoms and the colonial haptophyte *Phaeocystis antarctica* develop in response to increasing solar irradiance and mixed

*Email: ptortell@eos.ubc.ca

layer stratification (DiTullio & Smith 1996, Arrigo et al. 2000, Smith et al. 2000). High macronutrient concentrations, in combination with Fe input from melting sea ice (Sedwick & DiTullio 1997) and continental shelf sources (Gerringa et al. 2012), drive the accumulation of exceptionally high photosynthetic biomass (>20 µg chlorophyll *a* l^{-1} (µg chl *a* l^{-1})) and increased rates of carbon fixation (>2 g m^{-2} d^{-1}) in polynya waters (Arrigo & van Dijken 2003). The sea ice zone (SIZ) surrounding the polynyas also appears to host diverse and metabolically active algal populations (Stoecker et al. 2000, Kattner et al. 2004, Meiners et al. 2009), with chl *a* concentrations and photosynthetic rates that can be comparable to those in adjacent open waters. Collectively, polynya waters and the SIZ have been estimated to account for ~10% of total carbon fixation in the Southern Ocean (Arrigo et al. 1998), and these regions play a disproportionately important role in the biological export of organic carbon into sub-surface waters (Arrigo et al. 2008). Increasing attention has thus focused on understanding the factors that control phytoplankton productivity and CO_2 uptake in Southern Ocean polynya waters and surrounding sea ice.

To date, most phytoplankton studies in Antarctic polynyas have focused on sea ice cover, mixed layer depth and Fe supply as key environmental regulators of primary productivity and species assemblage composition (Arrigo et al. 2000, Smith et al. 2000, Arrigo et al. 2003b, Coale et al. 2003, Feng et al. 2010). In comparison, little is known about the potential effects of pCO_2 (partial pressure of CO_2) variability on phytoplankton ecology in these systems. Field studies in the Ross Sea, Weddell Sea and Amundsen Sea polynyas demonstrate extreme pCO_2 variability in polynya surface waters, with values ranging from ~500 ppm in early spring to ~100 ppm (i.e. <25% of atmospheric saturation) during periods of peak primary productivity (Bates et al. 1998, Sweeney et al. 2000, Tortell et al. 2011, Tortell et al. 2012). This pCO_2 variability is among the largest reported for any marine waters, yet very few studies have examined its potential influence on phytoplankton physiological ecology.

From a biochemical perspective, strong pCO_2 variability should exert a direct influence on phytoplankton photosynthesis given the low CO_2 affinity and turnover rate of ribulose-1,5-bisphosphate carboxylase/oxygenase (RubisCO) — the rate-limiting enzyme in the Calvin cycle (Badger et al. 1998). However, many phytoplankton employ carbon-concentrating mechanisms (CCMs) to increase CO_2 concentrations at the active site of RubisCO, thus increasing the efficiency of net C fixation (Giordano et al. 2005). Key elements of the CCM include the active uptake of CO_2 and/or HCO_3^- (the dominant form of inorganic carbon in sea water), and the activity of carbonic anhydrase (CA), which catalyzes the interconversion of CO_2 and HCO_3^- (Badger & Price 1994). CCM activity should influence cellular responses to pCO_2 variability (Riebesell 2004), and also exert a significant influence on photosynthetic C isotope fractionation (Laws et al. 2002), typically leading to ^{13}C enrichment of organic matter. This ^{13}C enrichment can result from the uptake of isotopically 'heavy' HCO_3^- (the $\delta^{13}C$ of HCO_3^- is ~10‰ lower than CO_2; Mook et al. 1974), or a reduction in cellular CO_2 efflux and greater relative photosynthetic consumption of internal CO_2 pools (Erez et al. 1998). Recent work has documented CCM expression by phytoplankton in the Ross Sea, where HCO_3^- accounts for ~80% of total photosynthetic inorganic carbon uptake, and membrane-bound extracellular CA (eCA) activity is widespread (Tortell et al. 2010). CCM activity in the Ross Sea appears to be regulated across *in situ* pCO_2 gradients (Tortell et al. 2010), and incubation experiments show significant CO_2-dependent shifts in primary productivity and phytoplankton species abundances (Tortell et al. 2008). These results suggest that pCO_2 can influence phytoplankton physiological ecology in Antarctic polynya waters, and the prevalence of CCM activity may help explain the higher $\delta^{13}C$ values of particulate organic carbon ($\delta^{13}C$-POC) previously observed in the Ross Sea (Villinski et al. 2000).

The extent to which results from the Ross Sea polynya can be extrapolated to other Antarctic polynyas is at present unknown due to a lack of relevant data. Moreover, virtually no information is available on the mechanisms of C utilization and CO_2 sensitivity of sea ice algal assemblages. Growth conditions in sea ice differ significantly from those of ice-free surface waters, and sea ice algae probably possess a distinct physiological ecology (Thomas & Dieckmann 2002). Of particular relevance to inorganic C acquisition, high productivity during the spring and summer melt season, coupled with reduced gas exchange within the semi-closed ice matrix, can lead to extreme CO_2 depletion (minimum values <1 µM, and a concomitant pH increase to values of ~10 (Gleitz et al. 1995, Delille et al. 2007, Papadimitriou et al. 2009). Stable C isotope data demonstrate a significant enrichment of ^{13}C in sea ice particulate organic matter during periods of active algal growth (Gibson et al. 1999, Kennedy et al. 2002, Papadimitriou et al. 2009, Munro et al. 2010), suggesting a restricted CO_2 supply

for C fixation and/or the uptake of ^{13}C-enriched HCO_3^-. Yet, very few studies have examined the physiological mechanisms of inorganic C uptake by sea ice algae (Gleitz et al. 1996, Mitchell & Beardall 1996), and no data are currently available for natural sea ice algal assemblages. This information is key to understanding the potential effects of CO_2 variability on sea ice primary production.

In this article, we report new measurements of inorganic C acquisition in Antarctic sea ice algae sampled between the West Antarctic Peninsula and the Ross Sea, and in surface phytoplankton assemblages sampled from polynya waters and the SIZ of the Amundsen Sea. This latter region has received relatively little research attention, despite its exceptionally high primary productivity (Arrigo & van Dijken 2003, Alderkamp et al. 2012, Arrigo et al. 2012) and strong CO_2 drawdown (Tortell et al. 2012). An important, and potentially unique, feature of the Amundsen Sea is the prevalence of glacial melt water associated with the inflow of relatively warm circumpolar deep water beneath the ice shelves (Walker et al. 2007, Jacobs et al. 2011). This melt water enhances Fe supply (Gerringa et al. 2012), influences the stability of the upper water column (Alderkamp et al. 2012), and plays a significant role in driving enhanced primary productivity in surface waters in the eastern part of the Amundsen Sea (Gerringa et al. 2012).

Our research goal was to characterize several fundamental aspects of the photoautotrophic C uptake system — HCO_3^- and CO_2 uptake capacity, eCA activity, C uptake kinetics and stable C isotope composition — in relation to environmental variables (e.g. CO_2) and phytoplankton taxonomic composition. To our knowledge, this work represents the first examination of C uptake by sea ice algal assemblages sampled *in situ*, and the first direct comparison of C uptake by sea ice and pelagic algae. This comparison provides insight into the unique physiological ecology of primary producers in contrasting polar habitats, and their potential responses to natural and anthropogenic perturbations of the high latitude C cycle.

MATERIALS AND METHODS

Sample collection

Sampling was conducted in the Amundsen Sea on the RV/IB '*Nathanial B. Palmer*' (cruise NBP 09-01) from January 11 to February 16, 2009, as part of the DynaLiFe program (Arrigo & Alderkamp 2012). We also sampled an extended transect through the sea ice zone between the West Antarctic peninsula and the Ross Sea on the IB '*Oden*' (cruise OSO 10-11) from December 8, 2010 to January 14, 2011. Fig. 1 shows the location of the sampling stations for both cruises, superimposed on mean sea ice concentrations derived from 12.5 km resolution Advanced Microwave Scanning Radiometer — Earth Observing System (AMSR-E) data (Cavalieri et al. 1990, updated 2006; http://nsidc.org/). During the 2009 Amundsen Sea cruise (hereafter referred to as Palmer), samples were collected from ice-free waters of the Amundsen and Pine Island polynyas, and from partially open waters in the sea ice zone

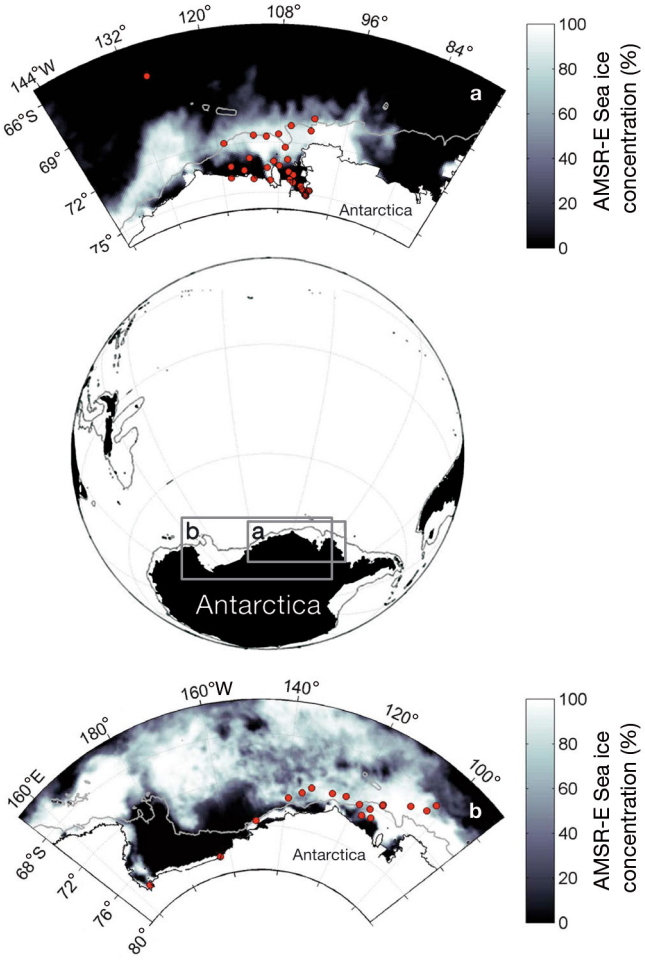

Fig. 1. Location of sampling stations (red circles) during (a) the Amundsen Sea Palmer expedition and (b) the Oden expedition. The background black and white scale represents the mean sea ice concentrations for each cruise, derived from the Advanced Microwave Scanning Radiometer — Earth Observing System (AMSR-E) satellite product (Cavalieri et al. 1990, updated 2006) with a spatial resolution of 12.5 km

north of the polynyas (Fig. 1a). One sampling station was located north of the sea ice zone (SIZ) in the open waters of the pelagic Southern Ocean (~66.5° S). In all cases, surface water (~10 m depth) was collected using Rosette sampling bottles mounted onto a frame with an attached CTD (conductivity, temperature, depth) sensor (Sea-Bird Electronics, SBE 911 plus).

During the 2010–2011 cruise (hereafter referred to as Oden), the majority of samples were collected from sea ice cores obtained using a 7.5 cm-diameter core barrel (Kovacs Mark 3) powered by an electric hand drill. Ice samples were collected from large floes to which the research vessel was moored. Before ice coring, snow thickness was measured at several positions in the immediate vicinity of the coring site. Cores extracted from the sea ice were immediately cut into 10 cm sections and placed in opaque 4 l polyethylene bottles containing 2 l of 0.2 µm filtered seawater. Individual core sections were then broken into smaller pieces and allowed to melt in the dark at room temperature. The melting process took ~12 h, during which sample temperatures remained close to 0°C. The addition of 0.2 µm filtered seawater to the melting ice ensured that salinities in the final samples were >8, thus minimizing osmotic shock on the algal populations. The bulk salinity of sea ice in the melted samples was calculated from the final salinity (measured using a refractometer) and volume of the melted samples. In samples used for chemical analysis (e.g. CO_2 concentrations), salinity was measured using a conductivity meter (WTW Cond 330i). Sea ice temperature was measured at 5 cm intervals immediately after the ice core was recovered using a digital thermistor with an accuracy of 0.1°C.

A number of additional samples from the Oden expedition were collected for comparison with ice core material. At several stations, we used a rigid inflatable boat (Zodiac) to sample floating sea ice with significant algal biomass (as judged qualitatively by the ice color). Small- to medium-size ice pieces were chipped off floating ice, placed in buckets with 2 l of 0.2 µm filtered seawater and allowed to melt in the dark as described above. We also collected several surface slush samples (below the snow layer), and one melt pond sample directly into polypropylene buckets. Slush samples were thawed in 0.2 µm filtered seawater as described above; melt-pond samples were used immediately. Finally, we collected seawater samples from 1 m below the ice/water interface, using a submersible pump (Rule bilge pump; 1500GPH).

Physiological assays

Material collected from the seawater and melted ice and slush samples was used in several physiological assays of inorganic C acquisition. Prior to the assays, phytoplankton were concentrated from samples by gentle filtration onto 47 mm diameter, 2.0 µm pore size, polycarbonate membranes. For the Palmer samples, 5–20 l of seawater was gravity filtered in a walk-in cold room (2°C). For melted sea ice and slush samples, 300 ml to 1 l of material was filtered under gentle vacuum (<100 mm Hg, 0.2 atm), ensuring that filters did not run dry. Phytoplankton were resuspended off the filters into one of the 3 seawater buffers used for experiments (see below, this section). In all cases, the buffers were made from 0.2 µm-filtered Southern Ocean water containing 10 mM N,N-bis(2-hydroxyethyl)glycine (Bicine) and stored at 4°C. A single batch of filtered Southern Ocean water was used for all experiments. Sub-samples of the concentrated cell suspensions were collected for chl *a* determinations (see 'Ancillary measurements' section) to normalize C uptake rates and eCA activities.

While pre-concentration of samples by filtration was necessary to achieve detection of enzyme activity and short-term ^{14}C uptake in our assays, this procedure can potentially introduce artifacts through taxon-specific decreases in cell viability. We tested for such effects by measuring photosynthetic efficiency, as determined by variable chl *a* fluorescence (F_v/F_m, where F_v is variable fluorescence and F_m is the maximum fluorescence yield in the dark), and by quantifying the abundance of major phytoplankton groups using photosynthetic pigments (see 'Ancillary measurements' section) before and after filtrations. In a limited set of experiments (n = 3), we observed a ~10–20% decrease in F_v/F_m after filtration, with the largest effects occurring in *Phaeocystis*-dominated phytoplankton assemblages. We also observed a ~10% reduction in *Phaeocystis*-specific pigments in concentrated samples relative to initial seawater samples. These observations suggest a discernible (though relatively modest) effect of our concentration procedure on cell physiological health, particularly for *Phaeocystis* and possibly other nanoflagellates.

The activity of eCA was determined in cell suspensions by measuring the rate of oxygen isotope exchange between $^{13}C^{18}O_2$ and $H^{13}C^{18}O_3^-$ in solution via membrane inlet mass spectrometry (Silverman 1982). Assays were conducted at pH 8.2 and 2°C in a thermostated cuvette coupled, via silicone mem-

brane inlet, to a quadropole mass spectrometer (Hiden Analytical HAL 3F, HPR 40). Full details of the experimental protocols for this assay can be found in Tortell et al. (2006). To quantify eCA activity, the rates of interconversion of HCO_3^- and CO_2 in cell suspensions were compared with those in cell-free buffer, and enzyme activity (U) was calculated as:

$$1\ U = S_c/S_u - 1 \quad (1)$$

where S_c and S_u refer to the catalyzed and uncatalyzed (i.e. cell free) rates of ^{18}O exchange, respectively. Using this formulation, one unit of activity reflects a 100% enhancement of the ^{18}O loss rate relative to the uncatalyzed value. In several instances, we used a membrane-impermeable CA inhibitor (dextran-bound sulfanilimide, DBS) to block CA activity in cell suspensions and provide a negative experimental control. As shown in Fig. 2, addition of 100 µM of DBS to our samples resulted in ^{18}O exchange rates that were not significantly different from those in cell-free buffers, confirming full inhibition of eCA activity.

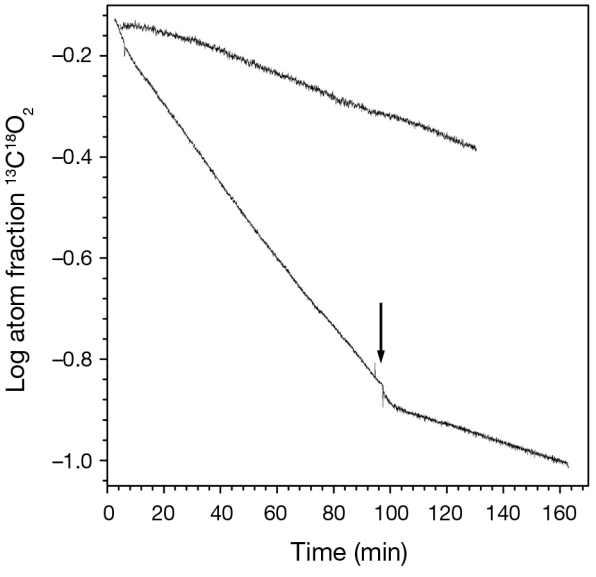

Fig. 2. Carbonic anhydrase catalyzed ^{18}O exchange between HCO_3^- and CO_2 in a sea ice algal assemblage (stn 10). During the assay, the relative proportion of double labeled CO_2 ($^{13}C^{18}O_2$) decreases exponentially due to equilibration with the large background $H_2{}^{16}O$ pool. Comparison of the slopes in the presence (lower line) and absence (blank; upper line) of a cell suspension provides a measure of extracellular carbonic anhydrase (eCA) activity. The arrow denotes the time when 100 µM dextran-bound sulfanilamide (DBS) was added to the sample chamber to inhibit eCA activity. The observed slope in DBS-treated cell suspensions is not significantly different from blank samples, indicating complete inhibition of eCA activity

The rate of C fixation derived from exogenous HCO_3^- and CO_2 uptake was determined using the isotope disequilibrium technique (Espie & Colman 1986), which has been described extensively (Elzenga et al. 2000, Tortell & Morel 2002, Martin & Tortell 2006). Briefly, the time course of ^{14}C fixation in a phytoplankton suspension is followed after the injection of a pH 7.0 ^{14}C spike solution to an assay buffer at pH 8.5. Cells fixing CO_2-derived C show significant curvature in the ^{14}C time course as the specific activity of the external CO_2 pool decreases exponentially during the experiment (due to re-equilibration of excess $^{14}CO_2$ with the bulk inorganic carbon pool). In contrast, the specific activity of the extracellular HCO_3^- and CO_3^{-2} pool remains virtually constant, resulting in near linear ^{14}C accumulation curves for cells fixing CO_2 derived from HCO_3^-. The amount of curvature in the ^{14}C fixation time course can thus be used as a measure of the relative contribution of exogenous HCO_3^- and CO_2 to total cellular C fixation. In these experiments, it is necessary to eliminate eCA activity to maintain the disequilibrium between HCO_3^- and CO_2 in solution. We used 100 µM DBS to specifically inhibit eCA (Fig. 2). Isotope disequilibrium experiments were run at 2°C and 200 µE m^{-2} s^{-1} full solar spectrum photosynthetically active irradiance (Rolf C. Hagen, Sun-Glo, 4200k), following the protocol described by Tortell et al. (2008). The resulting ^{14}C time course data were analyzed following the approach of Martin & Tortell (2006) to derive the relative fraction of HCO_3^--derived C fixation ($f_{HCO_3^-}$; range 0–1) from non-linear least-squares regression (SigmaPlot). At the pH of our assay buffer and spike solution, the model fits are only able to resolve $f_{HCO_3^-}$ values of 0.4 or greater. Given that eCA activity was blocked in our uptake experiments, we interpret our $f_{HCO_3^-}$ data in terms of HCO_3^- supply through direct membrane transport, rather than eCA-facilitated indirect HCO_3^- utilization (via extracellular dehydration to CO_2).

The substrate-dependent kinetics of C fixation (half-saturation constant, K_S, and biomass-normalized maximum C fixation rate, V_{max}) were also determined using a ^{14}C-based assay. In these assays, gross photosynthetic C fixation (incorporation of acid-stable organic ^{14}C compounds) was measured for 10 min over a range of external inorganic C concentrations in a pH 8.0 buffer. Experiments were conducted at 2°C and 200 µE m^{-2} s^{-1} full solar spectrum photosynthetically active irradiance. The experimental protocol for these assays has recently been described in detail (Tortell et al. 2010). Data from these experiments were analyzed using non-linear

regression (SigmaPlot) to fit the Michaelis–Menten hyperbolic equation and derive least-squares estimates for K_S and V_{max}:

$$V = V_{max} \times C/(C + K_S) \quad (2)$$

where V is the C uptake rate at any given external dissolved inorganic carbon (DIC) concentration, C.

Ancillary measurements

Additional samples were collected from sea ice assemblages and pelagic algal assemblages for bulk biochemical analyses. Sea ice algal material for these analyses was obtained from replicate cores (collected within a 1 m diameter circle), sectioned and melted as described under 'sample collection' above, while seawater phytoplankton samples (Palmer expedition) were collected from the replicate Niskin bottles. Samples for the determination of particulate organic carbon and particulate organic nitrogen (POC/N) and photosynthetic pigment concentrations were collected by gentle filtration onto glass fiber filters (GF/F, nominal pore size ~0.7 µm) and frozen at –80°C for subsequent laboratory analysis. Filters used for POC/N determinations were pre-combusted at 450°C for 4 h. POC/N concentrations were determined using an elemental analyzer coupled to an isotope ratio mass spectrometer at the UC Davis analytical laboratory. These analyses also yielded measurements of the isotopic ratios of $^{15}N/^{14}N$ and $^{13}C/^{12}C$ in samples.

Photosynthetic pigment concentrations in the Amundsen Sea samples were measured using high-pressure liquid chromatography (HPLC) following the protocols described by Alderkamp et al. (2012). We used the CHEMTAX algorithm (Mackey et al. 1996, Wright et al. 1996) to estimate the relative abundance of different phytoplankton taxa in our samples, based on several diagnostic pigments for individual classes (e.g. 19-hexanoyloxyfucoxanthin for *Phaeocystis antarctica* and fucoxanthin for diatoms). A full discussion of the CHEMTAX analysis for the Amundsen Sea samples is given in Alderkamp et al. (2012). Additional ship-board chl *a* measurements were conducted at sea by extraction from filtered samples overnight with 90% acetone and reading the chl *a*-specific fluorescence intensity, with an acidification step to correct for phaeopigments as described by Holm-Hansen et al. (1965).

For the Oden samples, algal material for photosynthetic pigment analysis was collected onto 47 mm GF/F filters (nominal pore size ~0.7 µm) by gentle vacuum (<100 mm Hg) and immediately frozen at –80°C for subsequent processing in our laboratory. In the laboratory, frozen samples were treated with 2–3 ml of 90% acetone and sonicated for 5 min to disrupt cells and extract pigments. The resulting crude pigment extract was filtered through a 0.2 µm polytetrafluoroethylene (PTFE) filter to remove cellular debris. A mixture of 250 µl filtered pigment extract, 50 µl deionized water, and 50 µl acetonitrile was injected into the reversed-phase C_8 column of the HPLC system (Waters Alliance BIO 2796 Bioseparations Module) and analyzed according to the protocol outlined in Zapata et al. (2000). We used a 2-solution gradient to elute pigments off the HLPC column into a photo-diode array detector: the first eluent was a 50:25:50 v:v:v mixture of methanol:acetonitrile: 0.25 M aqueous pyridine solution, and the second eluent was a 20:60:20 v:v:v mixture of methanol: acetonitrile:acetone. To calibrate pigment extraction yield, 10 µl of the pigment internal standard trans-β-Apo-8'-carotenal was added to each sample. Pigments were identified using a mixed pigments standard containing 23 different pigments dissolved in 90% acetone (DHI Water & Environment). Concentrations for each identified pigment were then quantified using standard curves generated for each individual pigment *a priori* to the HPLC runs.

Following sample processing, data were interpreted with the chemotaxonomy program CHEMTAX v.1.95, an updated version from that first presented in Mackey et al. (1996). The initial pigment ratio matrix used to initialize the iterative calculations was derived from a compilation of multiple field studies (Wright et al. 1996, Mackey et al. 1998, Rodriguez et al. 2002, Suzuki et al. 2002, Havskum et al. 2004, Vidussi et al. 2004, Miki et al. 2008, Fujiki et al. 2009, Kozlowski et al. 2011). In our analysis, we first examined whether the signature pigments for different phytoplankton groups were present in each sample. With this information, we assigned our samples to 2 major categories: one containing diatoms and prymnesiophytes only, and another potentially containing all of the major groups (i.e. diatoms, prymnesiophytes, dinoflagellates, chlorophytes, prasinophytes, cryptophytes and crysophytes). Based on the pigments detected in our samples and those associated to each phytoplankton group in the literature, we included the following pigments in our initial ratio table: chl c_3, magnesium 3,8-divinylphaeoporphyrin a5 monomethyl ester, chlorophyll c_2, peridinin, 19′-butanoyloxyfucoxanthin, fucoxanthin, prasinoxanthi, 19′-hexanoyloxyfucoxanthin, diadinoxanthin, alloxanthin, zeaxanthin, lutein, and chl *a*. To

avoid the potential for poor starting choices producing unrepresentative results, 60 iterations of the initial pigment ratios matrix were calculated. These matrices were obtained by random adjustments of each pigment ratio by ±35% and were applied to each sample separately, from which the best 10%, (lowest root mean square error), were used to calculate the mean percentage abundance of the algal groups. For most phytoplankton groups, other than crysophytes and prasinophytes, the final pigment ratios differed little from the range of values reported in the literature. Given that these phytoplankton groups did not account for a significant fraction of the community composition (<15% of total chl *a*) at the majority of stations, we did not attempt to improve their initial pigment ratio values.

During the Palmer cruise, pCO_2 in surface seawater samples was measured using underway membrane inlet mass spectrometry (MIMS). The full CO_2 data set from this expedition and a description of the analytical methods is presented elsewhere (Tortell et al. 2012). Bulk CO_2 concentrations (µmol kg^{-1}) in sea ice samples were calculated from measurements of pH, total alkalinity (A_T), temperature and salinity in discrete samples. Full details of the sampling, analytical methods and calculations can be found in Fransson et al. (2011). Briefly, ice core sections for CO_2 system measurements were transferred to gas-tight bags (Tedlar®) which were evacuated using a small vacuum pump and sealed. After samples had thawed in the dark at ~4°C, A_T was determined by potentiometric titration in an open cell with 0.05 M HCl, according to Haraldsson et al. (1997). pH was determined spectrophotometrically at 15°C (diode-array spectrophotometer, HP8453) using a 2 mM solution of the sulfonaphtalein dye, m-cresol purple, as an indicator (Clayton & Byrne 1993). The analytical precision was estimated to ±0.002 pH units, as determined by triplicate analysis of 1 sample every day. The pH of the indicator solution was measured daily using a 0.2 mm flow cell. The magnitude of the perturbation of seawater pH caused by the addition of the indicator solution was calculated and corrected for using the method described in Chierici et al. (1999). CO_2 concentrations in bulk ice-melt samples were calculated using CO2SYS (Pierrot et al. 2006) with pH and A_T as input parameters and the *in situ* ice temperature and measured salinity. We used the CO_2-system dissociation constants (K^*_1 and K^*_2) appropriate for freshwater samples estimated by Roy et al. (1993). The calculations were performed on the total hydrogen ion scale (pH_{tot}) using the HSO_4^- dissociation constant of Dickson (1990).

Samples for nutrient concentration measurements were collected from both CTD casts (Palmer cruise) and core sub-samples collected on the Oden expedition, and frozen for subsequent analysis. Samples were thawed in the laboratory and analyzed colorometrically using a Smart ChemTM 200 discrete analyzer (Westco Scientific Instruments) with standard colorimetric protocols for NO_3^- and HPO_4^{2-} (Grasshoff et al 1999). For the Oden samples, multiple (2 or 3) sub-samples (~12 cm^3) were removed from the middle of each ice core depth section using a hole saw connected to a hand drill. Sub-cores from each depth horizon were combined into a single 50 ml centrifuge tube and kept frozen until analysis.

Statistics

Variability among replicate samples was assessed based on standard deviations, and the statistical significance of differences between means based on *t*-test or ANOVA, with a threshold of $p < 0.05$. For C uptake parameters, standard errors were derived from non-linear regression using the Levenberg–Marquardt algorithm in SigmaPlot. Correlations between variables were assessed using Pearson's correlation coefficient.

RESULTS

Phytoplankton biomass and pCO_2 in the Amundsen Sea

The Amundsen Sea polynyas are bordered by a band of sea ice to the north and by ice shelves to the south, which include several major glaciers such as the Pine Island Glacier, Dotson ice shelf, Crosson ice shelf, and Getz Glacier. During our survey, dense phytoplankton blooms developed in surface waters of the Pine Island and the Amundsen polynyas, as described by Alderkamp et al. (2012). At the majority of sampling stations in both polynya waters and the sea ice zone, diatoms and *Phaeocystis antarctica* were the dominant phytoplankton taxa, accounting for an average 93% of the total chl *a* concentrations (based on CHEMTAX analysis; Alderkamp et al. 2012). *P. antarctica* was the dominant species at the majority of the sampling stations, accounting for more than 66% of the total chl *a* at 29 of the 44 stations we sampled. In contrast, diatoms dominated the phytoplankton assemblages at only 4 stations (>66% chl *a*). At 2 stations along the continental shelf break

Table 1. Characteristics of the Amundsen Sea sampling stations (Palmer cruise). The taxonomic composition of phytoplankton was derived from CHEMTAX analysis of photosynthetic pigments. Dashes indicate that a parameter was not measured

Stn	Latitude (°S)	Longitude (°W)	pCO_2 (µatm)	Chl *a* (µg l^{-1})	% diatom	% *Phaeocystis*	% other
3	70.462	101.933	400	0.4	29	23	44
5	71.188	102.364	384	0.7[a]	22	23	48
10	73.008	106.353	250	7.1	6	80	13
13	74.361	104.890	140	10.3	1	99	0
16	75.092	101.774	500	0.1	–	–	–
36	74.980	101.884	175	4.4	21	79	0
37	75.037	102.013	170	4.9	10	89	0
46	74.784	101.672	235	5.1	13	87	0
47	75.060	101.956	184	2.9	9	91	0
55	74.774	101.295	424	0.4	12	87	1
81	75.090	101.776	350	1.1	25	73	2
86	74.718	102.804	214	3.0	19	81	0
91	74.208	105.598	105	9.8	2	98	0
92	74.772	101.195	460	0.8	2	98	0
99	74.831	102.626	195	4.6	16	84	0
102	74.551	103.176	179	3.0	25	74	0
105	73.917	104.998	122	7.6	2	98	0
106	73.750	106.001	91	10.9	7	92	0
108	73.418	108.002	110	6.1	5	95	0
111	72.916	114.002	105	7.6	7	93	0
114	73.634	115.255	255	4.1	54	46	0
119	74.173	113.340	334	2.3	61	39	0
126	74.286	109.845	450	0.3	85	14	0
127	73.528	110.415	132	5.6	24	76	0
129	73.140	109.178	148	4.0	24	70	6
131	72.292	106.942	310	1.4	43	36	21
133	70.988	106.020	339	0.7	43	19	37
138	71.507	108.313	332	1.4	79	15	6
140	71.652	110.577	237	3.3	29	71	0
142	71.568	113.031	327	1.2	62	38	0
148	73.337	117.858	143	1.1	–	–	–
153	74.011	118.131	162	1.6	–	–	–
158	71.902	118.721	188	3.5	7	93	0
160	67.000	128.968	352	0.7	–	–	–

[a]This value may be underestimated as it yields a particulate organic C: chl *a* ratio of ~400, which is significantly higher than the mean value for other stations (119 ± 61)

(stns 3 and 5), cryptophytes and chlorophytes were also well represented in the phytoplankton assemblages, contributing ~40–50% of the total chl *a* (Table 1). The highest surface chl *a* (11 µg l^{-1}) was found in the Pine Island polynya (SE polynya depicted in Fig. 1a), where the phytoplankton assemblage was dominated by *P. antarctica*. This assemblage was sampled before and during the peak of phytoplankton biomass as indicated by remote-sensing chl *a* imagery (Alderkamp et al. 2012, Arrigo et al. 2012). Considerable spatial heterogeneity was observed in surface chl *a* in the Amundsen polynya (SW polynya in Fig. 1a), which was sampled approximately 1 wk after the peak of the phytoplankton bloom, and in the waters of the sea ice zone (SIZ) north of the open polynya. The lowest chl *a* concentrations across our survey (<1 µg l^{-1}) were observed in the northeast region of the SIZ.

Across all sampling sites in the Amundsen Sea, surface water pCO_2 ranged from ~90 to 500 ppm (Tortell et al. 2012). There was a significant negative correlation between pCO_2 and chl *a* concentrations ($r = -0.82$, $p < 0.0001$, $n = 29$, data not shown), indicating significant biological CO_2 uptake in surface waters. The lowest pCO_2 waters occurred at water stations with high *Phaeocystis antarctica* abundance in the Pine Island polynya.

C uptake by Amundsen Sea phytoplankton

Representative ^{14}C uptake data used to derive phytoplankton C uptake parameters are shown in Fig. 3, while Table 2 shows the quantitative results of all C uptake assays and eCA activity measurements. With the exception of one sampling site (stn 111 in the SIZ boarding the Amundsen polynya), HCO_3^- was a significant source of inorganic C taken up by all of the phytoplankton assemblages sampled from Amundsen Sea. The average $f_{HCO_3^-}$ was 0.61 ± 0.11 (i.e. ~60% of fixed C derived from extracellular HCO_3^-), with a range of <0.40 to 0.82. The lowest $f_{HCO_3^-}$ we measured (<0.4 at stn 111) cannot be accurately quantified given the non-linear behavior of the curve-fitting equations (see 'Materials and methods'). We detected significant eCA levels in all of the Amundsen Sea samples we examined on the Palmer cruise. eCA activity ranged from 2.81 to 16.3 U (µg chl *a*)$^{-1}$ (see Eq. (1) for the calculation of U) with a mean value of 6.54 ± 2.61 (Table 2). This mean activity translates into a ~650% enhancement of CO_2 and HCO_3^- exchange rates relative to the uncatalzyed reaction. There were no significant correlations between eCA activity and pCO_2 or phytoplankton taxonomy ($r < 0.2$). Similarly, $f_{HCO_3^-}$ was not correlated to either of these variables ($r < 0.2$).

We observed saturation kinetics of short-term C fixation in the Amundsen Sea phytoplankton assem-

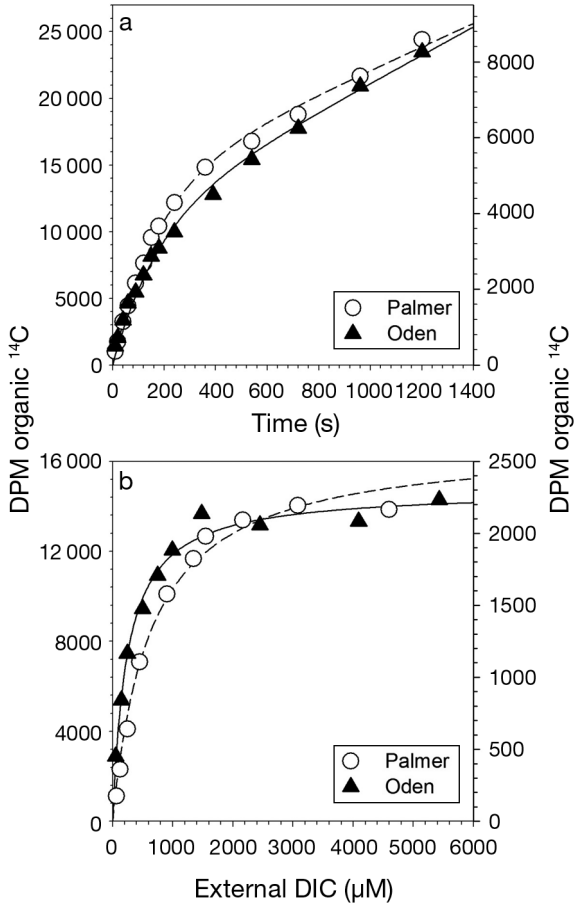

Fig. 3. Representative ^{14}C uptake curves obtained with sea ice algae (black triangles) and open-water phytoplankton (white circles) from the Oden and Palmer expeditions (Stns 30 and 133, respectively). Panel (a) shows results from isotope disequilibrium experiments and panel (b) shows results of C substrate affinity measurements. Lines on the plots represent non-linear least squares regression equations fit to the data as described by Martin & Tortell (2006). Note the difference in *y* axis scales for the 2 plots. The left-hand axis is used for the Palmer data in both panels. DPM is dissolved particulate matter, DIC is dissolved inorganic carbon

blages (Fig. 3b), and were able to obtain good fits of the Michaelis–Menten hyperbolic equation to our ^{14}C fixation data. Least-squares regression estimates for V_{max} and K_S are presented in Table 2. V_{max} ranged from 0.3 to 4.1 mg C (mg chl *a*)$^{-1}$ h^{-1} with a mean value of 0.79 ± 0.66 mg C (mg chl *a*)$^{-1}$ h^{-1}. K_S for inorganic C ranged from 234 to 3646 µM, with a mean value of 776 ± 596 µM. There was a significant positive correlation between *in situ* pCO_2 and K_S of Amundsen Sea phytoplankton assemblages (Fig. 4; r = 0.69, p < 0.0001). This result indicates a greater cellular C affinity (i.e. lower K_S) in low pCO_2 waters. We also observed a positive correlation between pCO_2 and V_{max}, but the strength of this correlation (r = 0.37) was much weaker than that observed with K_S. Both V_{max} and K_S exhibited weak, but significant, negative correlations with relative *Phaeocystis* abundance (r = −0.56 and r = −0.4, respectively, p < 0.05), suggesting higher C uptake affinity and lower maximum C transport rates in *Phaeocystis*-dominated assemblages.

To summarize the results presented above, we observed evidence of widespread CCM activity in Amundsen Sea phytoplankton assemblages. All but one of the phytoplankton assemblages showed a significant capacity for HCO_3^- uptake, and eCA activity was readily detected in all samples. K_S for C fixation was, in most cases, significantly lower than ambient inorganic C concentrations in seawater, suggesting the presence of a transport-mediated C uptake system. We observed a significant trend in C fixation kinetics across natural pCO_2 gradients, with higher substrate affinity (i.e. low K_S) in low pCO_2 waters. This pCO_2-dependent trend may have driven the apparent weak tendency for lower K_S and V_{max} in *Phaeocystis*-dominated waters.

Biological and chemical characteristics of the sea ice sampling stations

At the time of our sampling on board the Oden cruise (late December 2010 to mid January 2011), ice temperatures were generally close to the freezing point of seawater (mean −1.3 ± 0.43°C) and showed relatively little depth variability within the cores (data not shown). Nutrient concentrations, measured in bulk ice-melt samples, were also consistently low across all samples (data not shown), with NO_3^- levels typically <1 µM. Significant variability was observed, however, in phytoplankton biomass (bulk chl *a*) across sampling stations and in depth profiles from individual ice cores (Fig. 5). In the samples used for physiological assays, chl *a* concentrations ranged over 2 orders of magnitude from <1 µg l^{-1} (bulk ice concentration) to ~250 µg l^{-1} (Table 3, Fig. 5). Many stations (e.g. Stns 31, 32 and 41) exhibited a pronounced chl *a* maximum at the bottom of the ice core, in close proximity to the ice/water interface (Fig. 5). In some cases, however, the highest apparent phytoplankton biomass was located close to the top of the ice core (e.g. Stns 1 and 2; Fig. 5). Several stations showed maximum chl *a* concentrations at a mid-core depth (e.g. Stns 25, 27). In all cases, chl *a* concentrations in the seawater below the ice (larger filled circles in Fig. 5) were substantially lower than those in the bottom ice layer. For slush samples (filled tri-

Table 2. C uptake parameters and stable isotope composition of particulate organic carbon of the Amundsen Sea phytoplankton assemblages (Palmer cruise). Errors (±) represent standard error estimates for parameters derived from model fits to data. $f_{HCO_3^-}$ is the relative fraction of HCO_3^--derived C fixation, V_{max} is biomass-normalized maximum C fixation rate, K_S is the half-saturation constant, eCA is extracellular carbonic anhydrase and δ^{13}C-POC is the C isotope composition of particulate organic carbon. Dashes indicate that a parameter was not measured

Stn	$f_{HCO_3^-}$	V_{max} (mg C (mg chl *a*)$^{-1}$ h^{-1})	K_S (µM)	eCA activity (U (µg chl *a*)$^{-1}$)	δ^{13}C-POC (‰)
3	0.63 ± 0.02	1.77 ± 0.07	756 ± 107	9.3	–27.97
5	0.65 ± 0.02	4.10 ± 0.13[a]	1264 ± 101	8.1	–28.32
10	0.82 ± 0.01	0.61 ± 0.03	709 ± 108	6.4	–29.14
13	0.79 ± 0.02	0.25 ± 0.02	234 ± 104	9.5	–27.98
16	–	0.67 ± 0.11	3646 ± 1444	–	–26.88
36	0.67 ± 0.06	0.27 ± 0.02	377 ± 168	6.9	–27.85
37	0.63 ± 0.03	0.79 ± 0.06	537 ± 154	10.0	–27.57
46	0.56 ± 0.02	0.47 ± 0.02	692 ± 115	4.3	–27.49
47	0.65 ± 0.03	0.50 ± 0.03	531 ± 138	5.6	–27.74
55	–	0.55 ± 0.04	754 ± 164	–	–28.21
81	–	0.64 ± 0.02	1179 ± 109	–	–29.29
86	0.60 ± 0.02	–	–	2.8	–
91	0.74 ± 0.02	0.54 ± 0.06	308 ± 141	5.1	–26.65
92	–	0.86 ± 0.14	1541 ± 812	–	–
99	0.77 ± 0.01	0.71 ± 0.06	648 ± 161	7.0	–27.63
102	0.63 ± 0.03	0.43 ± 0.01	437 ± 65	4.4	–27.27
105	0.56 ± 0.02	0.42 ± 0.02	373 ± 106	4.9	–26.64
106	0.70 ± 0.03	0.64 ± 0.03	728 ± 117	–	–26.66
108	–	0.64 ± 0.04	485 ± 122	7.6	–26.52
111	<0.40	0.62 ± 0.05	376 ± 136	5.1	–26.60
114	0.55 ± 0.04	0.83 ± 0.06	687 ± 156	4.0	–26.47
119	0.42 ± 0.03	1.06 ± 0.04	902 ± 94	5.1	–27.99
126	0.49 ± 0.02	–	–	4.7	–26.31
127	0.46 ± 0.04	0.65 ± 0.02	584 ± 70	4.0	–27.17
129	0.56 ± 0.02	0.51 ± 0.03	435 ± 80	5.2	–26.66
131	0.67 ± 0.01	0.92 ± 0.05	802 ± 117	6.7	–27.79
133	0.68 ± 0.01	0.96 ± 0.04	631 ± 73	8.7	–27.21
138	0.46 ± 0.03	0.89 ± 0.07	934 ± 213	7.4	–29.98
140	0.42 ± 0.03	0.74 ± 0.03	688 ± 83	6.0	–28.73
142	0.68 ± 0.01	0.71 ± 0.04	824 ± 143	7.3	–28.63
148	0.63 ± 0.02	0.62 ± 0.02	1001 ± 99	6.4	–25.64
153	0.42 ± 0.04	0.86 ± 0.06	743 ± 161	6.5	–24.63
158	0.65 ± 0.02	0.65 ± 0.05	464 ± 124	4.3	–29.30
160	0.61 ± 0.02	0.38 ± 0.02	560 ± 140	16.4	–28.20

[a]This high value may result from underestimation of the chl *a* concentration at this station

angles in Fig. 5), we observed chl *a* concentrations that were similar (e.g. Stn 2), higher (e.g. Stn 27), or lower (e.g. Stn 3) than those observed in the top of the ice core.

As observed in the Amundsen Sea (Palmer cruise) samples, diatoms and *Phaeocystis antarctica* accounted for the majority of phytoplankton (>90%) in most of the Oden sea ice samples (20 out of 26; Table 3). Diatoms were the dominant taxonomic group in the majority of ice core samples we collected, although high *Phaeocystis* abundance (>50% of total chl *a*) was observed at 4 sampling stations. At several stations, cryptophytes also comprised a significant component of the microalgal assemblages, with a maximum relative abundance of ~60% at Stn 33. Prasinophytes were observed in 3 samples, but their relative abundance never exceeded 15%.

Bulk CO_2 concentrations in the Oden sea ice samples were highly variable, ranging from ~0.1 to 30 µmol kg^{-1}. Seawater interface samples (n = 3) showed the highest and most uniform CO_2 concentrations (mean = 27.5 ± 1.8 µmol kg^{-1}), with an equivalent pCO_2 of 403 ± 26 µatm. In slush samples (n = 3), mean CO_2 concentrations were 2.9 ± 0.76 µmol kg^{-1}, while ice core samples exhibited a mean CO_2 concentration of 5.3 ± 6.9 µmol kg^{-1} (range 0.1–17.4 µmol kg^{-1}).

Carbon uptake by sea ice algal assemblages

We obtained good results from both isotope disequilibrium experiments and C fixation kinetic assays with the sea ice algae (Fig. 3a,b), and were able to obtain robust curve fits to our ^{14}C data. Parameter values for $f_{HCO_3^-}$, V_{max}, K_S and eCA activity obtained for the sea ice algal assemblages are presented in Table 4. Due to relatively small sample sizes and high variability, there were no clear differences in any of these parameters among the various sample types (i.e. ice cores, seawater, floating ice, slush or melt ponds; ANOVA, $p > 0.1$). We have thus combined all the Oden samples (except ice covered seawater) in our discussion of C uptake/fixation in sea ice algae.

$f_{HCO_3^-}$ in the sea ice algal assemblages ranged from <0.40 to 0.87 (mean = 0.66 ± 0.19). Short-term V_{max} ranged from 0.03 to 6.19 mg C (mg chl *a*)$^{-1}$ h^{-1} (mean = 0.52 ± 1.3 mg C (mg chl *a*)$^{-1}$ h^{-1}), while K_S ranged from 103 to 5376 µM (mean = 1239 ± 1479 µM; Table 4). Relatively low eCA activity was detected in most sea ice algal samples. The activity of eCA ranged from 0.2 to 6.5 U (µg chl *a*)$^{-1}$ (mean =

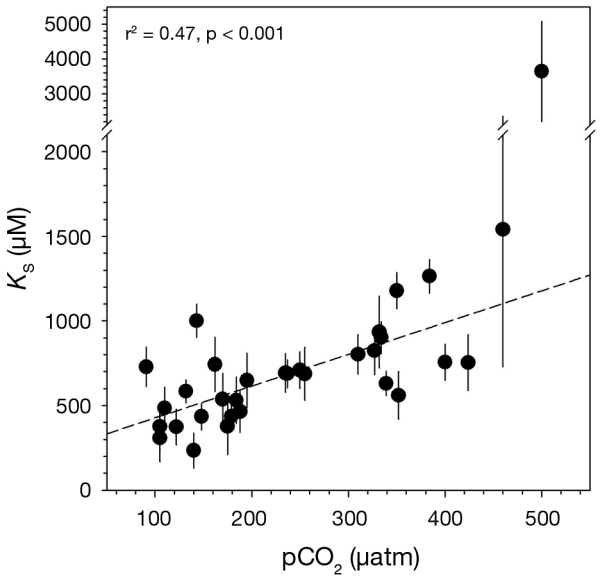

Fig. 4. Relationship between *in situ* pCO_2 and the half-saturation constant (K_S) for short-term C fixation in surface water phytoplankton assemblages in the Amundsen Sea. Error bars represent the standard error. K_S values obtained from non-linear curve fits

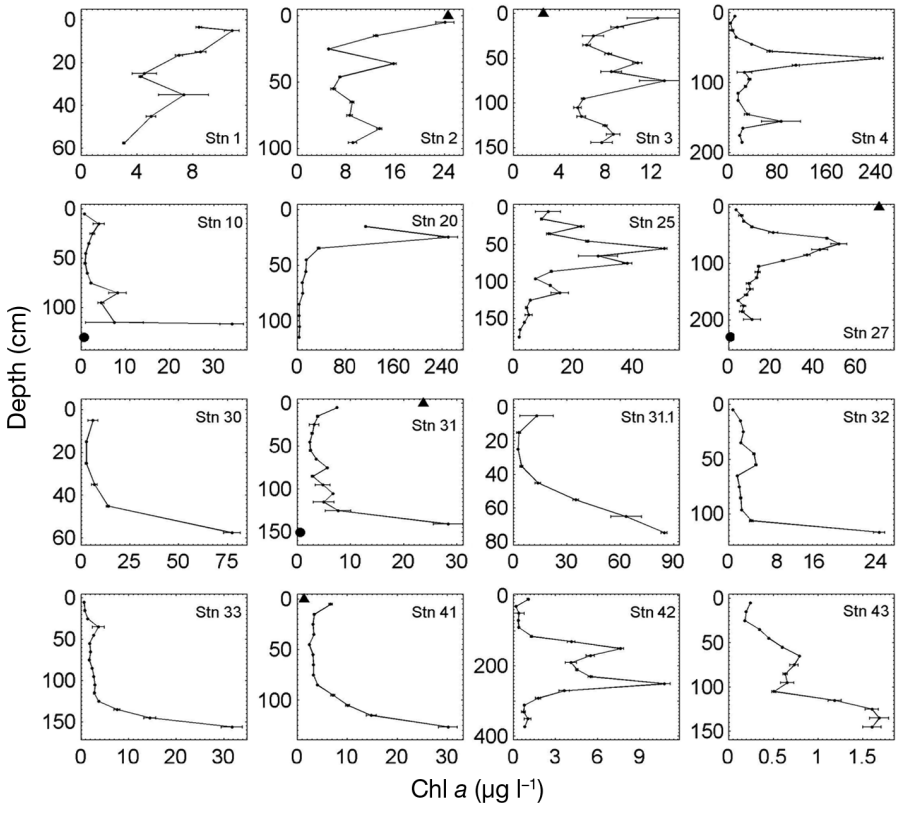

Fig. 5. Depth profiles of chl *a* concentrations in sea ice cores sampled on the Oden expedition, representing measurements taken from biomass ice cores sectioned every 10 cm. Slush and seawater/ice interface samples are shown as black triangles and circles, respectively. Note that *x* and *y* scales differ among the various sub-plots. Error bars represent standard deviation of duplicate or triplicate chl *a* measurements

1.6 ± 1.6 U (µg chl *a*)$^{-1}$). There were no statistically significant correlations between bulk sea ice CO_2 concentrations or algal taxonomic composition and any of the C uptake parameters we measured.

Comparison of carbon uptake by sea ice algae and phytoplankton

A direct comparison of C uptake parameters measured in phytoplankton and sea ice algal assemblages (Fig. 6) shows that there were no statistically significant differences (*t*-test, $p > 0.1$) in $f_{HCO_3^-}$ between the 2 groups. Indeed, the range and mean value of $f_{HCO_3^-}$ were virtually identical for the 2 data sets (Fig. 6a). Similarly, we did not detect a statistically significant difference in C fixation kinetics (either K_S or V_{max}) between sea ice algae and phytoplankton, despite a tendency towards higher mean V_{max} in the phytoplankton assemblages (Fig. 6b,c). We did, however, observe significantly higher eCA activity in phytoplankton assemblages relative to sea ice algae (*t*-test, $t = 8.12$, $p < 0.001$, Fig. 6d). This was the only statistical difference in C uptake parameters detected between algae in the 2 habitats.

Stable C isotope signatures

Isotopic analysis of particulate material from our Amundsen Sea samples showed moderate variability in $\delta^{13}C$ (i.e. $^{13}C/^{12}C$ ratios) in surface water phytoplankton assemblages, with values ranging from −24.6 to −30‰ (mean −27.7 ± 1.1‰; Table 2). These $\delta^{13}C$ values were not correlated to $f_{HCO_3^-}$ or any of the other phytoplankton C uptake parameters we measured. We did, however, observe a relationship between $\delta^{13}C$–POC and the ratio of C uptake rates to CO_2 concentrations (no significant relationship was observed to either uptake rate or CO_2 alone). For this analysis, we converted our V_{max} values (Table 2) into potential growth rates (µ′; d^{-1}), by normalizing to a nominal C:chl *a* ratio of 100 g:g (Alderkamp et

Table 3. Characteristics of sea ice sampling stations (Oden cruise). Dashes indicate that a parameter was not measured

Stn	Sample type	Latitude (°S)	Longitude (°W)	Ice sampling depth (cm)	Snow depth (cm)	chl *a* (µg l^{-1})	CO_2 (µM)	% diatom	% *Phaeocystis*	% other
1	Ice core	68.591	102.135	60	28	2.9	2.7	100	0	0
2	Slush layer	69.469	103.076	0	33	24.6	2.7	86	14	0
3	Slush layer	70.030	106.951	0	41	2.6	–	87	13	0
4	Ice core	71.242	113.155	60	38	194.7	17.4	83	2	15
5	Ice core	71.316	113.151	95	37	–	1.7	95	5	0
10a	Ice core	72.776	114.174	120	35	72.1	2.1	96	4	0
10b	Seawater interface	72.776	114.174	130	35	0.7	25.7	100	0	0
10c	Floating ice	72.776	114.174	0	0	109.9	–	52	12	36
20	Ice core	72.124	115.602	25	48	245.2	–	84	16	0
25	Ice core	72.963	116.973	170	52	3.0	0.5	88	12	0
27a	Seawater interface	72.184	118.951	230	58	0.8	27.6	100	0	0
27b	Ice core	72.184	118.951	10	58	3.4	16.1	94	6	0
27c	Slush layer	72.184	118.951	0	58	70.6	2.2	94	6	0
27d	Floating ice	72.184	118.951	0	0	71.7	–	70	30	0
30	Ice core	72.035	123.178	55	20	47.9	0.5	97	3	0
31a	Seawater interface	72.171	127.090	150	31	0.5	29.2	45	55	0
31b	Ice core	72.171	127.090	10	31	14.6	1.0	6	94	0
31c	Slush layer	72.171	127.090	0	31	23.7	–	6	94	0
31d	Floating ice	72.171	127.090	0	0	155.9	–	99	1	0
31h	Ice core	72.221	133.151	70	10	84.6	–	82	2	16
32a	Ice core	72.808	135.569	110	15	40.8	–	96	4	0
32b	Melt pond	72.808	135.569	0	0	35.3	–	45	55	0
33	Ice core	73.418	139.301	155	6	31.7	0.1	23	21	57
41a	Slush layer	75.551	149.310	0	15	1.4	3.7	45	4	51
41b	Ice core	75.551	149.310	130	15	8.9	1.8	89	0	11
43	Ice core	77.494	–165.713	140	3	2.6	14.3	96	4	0

Table 4. C uptake parameters and stable isotope composition of particulate organic carbon for sea ice algae (Oden cruise). Dashes indicate that a parameter was not measured. Errors (±) represent standard error estimates for parameters derived from model fits to data. $f_{HCO_3^-}$ is the relative fraction of HCO_3^--derived C fixation, V_{max} is biomass-normalized maximum C fixation rate, K_S is the half-saturation constant, eCA is extracellular carbonic anhydrase and δ^{13}C-POC is the C isotope composition of particulate organic carbon

Stn	Sample type	$f_{HCO_3^-}$	V_{max} (mg C (mg chl *a*)$^{-1}$ h^{-1})	K_S (µM)	eCA activity (U (µg chl *a*)$^{-1}$)	δ^{13}C-POC (‰)
1	Ice core	–	6.19 ± 0.489	5376 ± 661	2.8	–22.53
2	Slush layer	–	0.03 ± 0.004	2776 ± 734	–	–19.73
3	Slush layer	0.11 ± 0.23	–	–	2.5	–19.01
4	Ice core	0.74 ± 0.01	0.22 ± 0.013	2394 ± 302	0.9	–20.43
5	Ice core	0.74 ± 0.02	0.34 ± 0.032	4998 ± 777	0.8	–20.22
10a	Ice core	0.72 ± 0.01	0.20 ± 0.006	642 ± 63	0.2	–17.24
10b	Seawater interface	–	0.78 ± 0.051	625 ± 135	1.2	–25.65
10c	Floating ice	0.87 ± 0.01	0.03 ± 0.002	1260 ± 221	0.8	–20.54
20	Ice core	0.46 ± 0.03	–	–	0.6	–17.36
25	Ice core	0.44 ± 0.06	0.28 ± 0.051	2073 ± 832	0.2	–19.32
27a	Seawater interface	0.68 ± 0.02	–	–	1.9	–22.92
27b	Ice core	0.56 ± 0.05	0.16 ± 0.012	1348 ± 259	0.2	–24.06
27c	Slush layer	0.84 ± 0.01	0.08 ± 0.003	149 ± 28	1.1	–15.98
27d	Floating ice	0.82 ± 0.01	0.49 ± 0.017	344 ± 46	1.3	–21.12
30	Ice core	0.79 ± 0.01	0.08 ± 0.002	252 ± 25	0.7	–19.61
31a	Seawater interface	0.72 ± 0.02	0.43 ± 0.029	1104 ± 209	1.7	–18.41
31b	Ice core	–	0.08 ± 0.004	941 ± 137	2.9	–20.95
31c	Slush layer	<0.40	0.08 ± 0.004	897 ± 144	2.2	–17.15
31d	Floating ice	0.86 ± 0.01	0.22 ± 0.008	246 ± 42	0.7	–19.38
31h	Ice core	0.61 ± 0.02	–	292 ± 40	0.2	–19.39
32a	Ice core	0.75 ± 0.03	0.03 ± 0.001	138 ± 26	0.6	–12.85
32b	Melt pond	0.67 ± 0.02	0.10 ± 0.001	297 ± 18	5.7	–14.17
33	Ice core	0.81 ± 0.02	0.06 ± 0.003	103 ± 31	0.7	–12.92
41a	Slush layer	0.70 ± 0.03	–	–	–	–21.21
41b	Ice core	0.61 ± 0.01	0.06 ± 0.004	436 ± 115	0.7	–20.30
43	Ice core	0.35 ± 0.05	1.05 ± 0.056	564 ± 106	6.6	–22.89

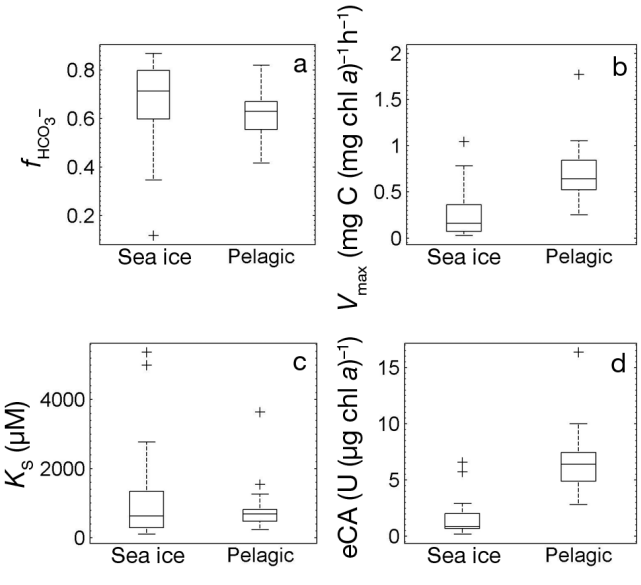

Fig. 6. Summary comparison of C uptake parameters for the Oden (sea ice) and Palmer (pelagic) algal assemblages: (a) the relative fraction of HCO_3^--derived C fixation ($f_{HCO_3^-}$), (b) the biomass-normalized maximum C fixation rate (V_{max}), (c) the half-saturation constant (K_S) and (d) the extracellular carbonic anhydrase activity (eCA). The central bar in the boxes represents the median value and the top and bottom of the boxes represent the 75th and 25th percentiles, respectively. Error bars extend to the 95% confidence intervals; +: outliers. Note that in panel (b) 2 points with V_{max} > 2 mg C (mg chl *a*)$^{-1}$ h^{-1} have been omitted for greater visual clarity. The corresponding data are, however, included in Tables 2 & 4

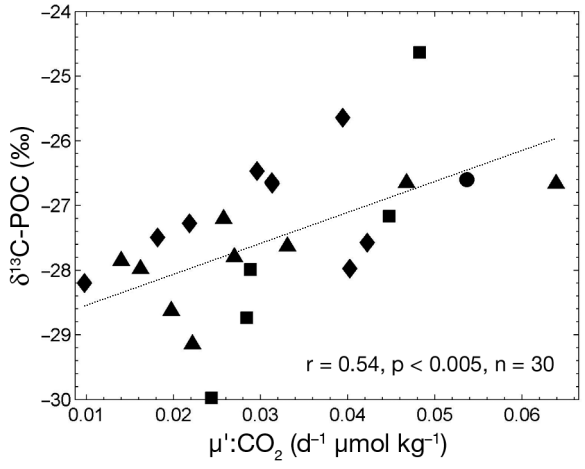

Fig. 7. Relationship between C isotope composition of particulate organic carbon ($\delta^{13}C$–POC) and the ratio of potential growth rates (µ′) to CO_2 concentrations in surface waters of the Amundsen Sea. Potential growth rates were derived from ^{14}C measurements of dissolved inorganic carbon-saturated C fixation rates (V_{max}, mg C (mg chl *a*)$^{-1}$ h^{-1}; see Table 2) using a nominal C:chl *a* ratio of 100 (Alderkamp et al. 2012). The different symbols represent $f_{HCO_3^-}$ ranges: ●, <0.4; ■, 0.6–0.7; ◆, 0.7–0.8; ▲, 0.8–0.95

al. 2012). The resulting ratio of µ′:CO_2 provides a measure of the relative C demand/supply ratio, as described previously (e.g. Laws et al. 1995). The µ′:CO_2 ratio was positively correlated (r = 0.54, p < 0.005, n = 30) to $\delta^{13}C$, indicating heavier C isotope signatures, and potentially lower C isotope fractionation, under conditions of higher carbon demand and/or lower CO_2 supply (Fig. 7).

Relative to the phytoplankton assemblages, sea ice algae showed significantly heavier C isotope signatures (i.e. greater ^{13}C enrichment) and more variable $\delta^{13}C$-POC, with values ranging from −25.65 to −12.85‰ (mean −19.4 ± 3.1; Table 4). Without direct measurements of $\delta^{13}C$ of the dissolved inorganic C pool, we cannot directly determine whether these heavy $\delta^{13}C$ values resulted from a ^{13}C-enriched inorganic carbon source (produced by Raleigh distillation in a semi-closed system) or from a decrease in photosynthetic isotope fractionation per se. As with the surface water phytoplankton samples, we found no statistically significant relationship between the $\delta^{13}C$ values of the sea ice algae and any other measured biological or chemical parameter (e.g. chl *a*, $f_{HCO_3^-}$ or eCA). Nor did we observe any significant relationship between sea ice algal $\delta^{13}C$ and the ratio of C uptake to CO_2 concentration (µ′:CO_2).

DISCUSSION

While it is now clear that primary productivity exerts a major control on CO_2 cycling in Antarctic continental shelf waters (Arrigo et al. 2008) and sea ice (Fransson et al. 2011), the extent to which CO_2 variability influences phytoplankton physiological ecology in these systems remains largely unexplored. To address this question, our field study examined the mechanisms of inorganic C uptake by sea ice algae and phytoplankton across several Southern Ocean polynyas. Specifically, we sought to quantify the capacity for photosynthetic uptake of CO_2 vs. HCO_3^-, the substrate-dependent kinetics of C fixation, the activity levels of eCA and the influence of algal taxonomic composition and external CO_2 concentrations on CCM activity. To our knowledge, there are only 2 previous reports of phytoplankton CCMs in polynya waters (Tortell et al. 2008, Tortell et al. 2010), and no previous characterization of C uptake physiology in natural sea ice algal assemblages. The results presented here thus contribute significantly to a small body of existing data.

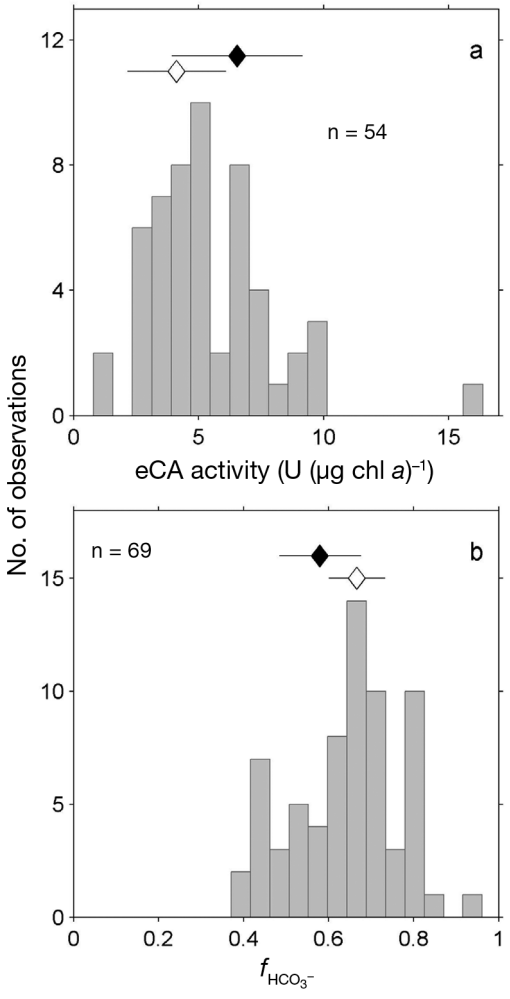

Fig. 8. Compilation of (a) eCA activity and (b) $f_{HCO_3^-}$ measurements for phytoplankton assemblages in the Ross and Amundsen seas. Open diamonds represent mean (±SD) of all Ross Sea measurements (Tortell et al. 2010, plotted along the *x* axis) and black diamonds represent the mean (±SD) of the Amundsen Sea data (this study). The position of the diamonds along the *y* axis is arbitrary and chosen for greatest visual clarity

Phytoplankton C uptake across Antarctic polynyas

Compiling all of the available C uptake data from the Ross Sea (Tortell et al. 2010) and Amundsen Sea (this study; Fig. 8), we can assess the variability in $f_{HCO_3^-}$ and eCA across more than 50 phytoplankton samples from Southern Ocean polynyas. This comparison illustrates that eCA and $f_{HCO_3^-}$ do not differ statistically between the Ross and Amundsen seas (Fig. 8), and provides strong evidence for widespread HCO_3^- transport and CCM activity in Antarctic polynya waters. Riebesell et al. (1993) originally suggested that slow CO_2 diffusion rates could limit the growth of Antarctic phytoplankton in the absence of a cellular HCO_3^- transport system. These authors reported reduced growth rates in the polar diatom *Rhizosolenia cf. alata* at CO_2 concentrations <20 µM, and showed that DIC uptake rates in this species did not exceed the calculated CO_2 diffusive supply. In contrast, our results, and those of other studies (Cassar et al. 2004, Neven et al. 2011), suggest that HCO_3^- utilization is prevalent in Antarctic waters, and argue strongly against widespread CO_2 diffusion limitation of phytoplankton growth in the Southern Ocean.

HCO_3^- utilization by phytoplankton is believed to require CA catalysis to maintain high rates of CO_2 delivery to RubisCO. This CA activity can occur either extracellularly, as part of the C transport system, or in one or more intracellular compartments. We were able to detect eCA-catalyzed interconversion of CO_2 and HCO_3^- in all of the Amundsen Sea surface water phytoplankton assemblages, yet activities were relatively low compared with that observed in a number of laboratory studies (e.g. Rost et al. 2003) and did not exhibit any apparent CO_2-dependent regulation or differences across phytoplankton taxonomic groups. The lack of a taxonomic effect on eCA activity stands in contrast to recent observations from the Ross and Bering seas, where increased eCA activity was observed in diatom-dominated phytoplankton assemblages, relative to assemblages dominated by various nanoflagellates (including *Phaeocystis*). At least part of this discrepancy may be attributable to the strong dominance of *Phaeocystis antarctica* and a low prevalence of diatoms in most Amundsen Sea phytoplankton assemblages we sampled. The low, and apparently constitutive, eCA levels we measured probably reflect the dominance of direct HCO_3^- transport as a mode of inorganic C uptake across all pCO_2 levels in the Amundsen Sea. In contrast, higher and potentially CO_2-dependent activity would be expected for intracellular CA, which acts to dehydrate HCO_3^- to deliver CO_2 at the site of C fixation by RubisCO. Such intracellular activity was not measured in our study.

C fixation kinetics in polynya waters

As we have previously observed in polynya waters of the Ross Sea (Tortell et al. 2010), surface water phytoplankton in the Amundsen Sea exhibited substrate-dependent saturation kinetics of ^{14}C fixation. In both these polynyas, K_S for phytoplankton assemblages (358 ± 43 µM and 776 ± 105, for the Ross and

Amundsen seas, respectively) are well below the inorganic C concentrations in Southern Ocean waters (> 2100 µM). When expressed in terms of CO_2 concentrations (assuming that ~1% of the inorganic carbon pool exists as CO_2), these mean K_S values (~4 and 8 µM) are also lower than the K_S of purified algal RubisCO (range ~10 to 60 µm; Badger et al. 1998). The discrepancy between the cellular kinetics of C fixation *in vivo* and the kinetics of isolated RubisCO provides strong evidence for the accumulation of high intracellular CO_2 levels, which is a defining characteristic of the CCM (Badger et al. 1998).

Unlike $f_{HCO_3^-}$ and eCA activity, cellular C fixation kinetics appear to differ significantly between the Ross and Amundsen seas. The mean K_S value was nearly 2-fold higher in the Amundsen Sea phytoplankton assemblages (776 vs. 358 µM), while the mean V_{max} value was nearly 5-fold higher (0.79 ± 0.12 vs. 0.16 ± 0.02 mg C (mg chl *a*)$^{-1}$ h^{-1}). As shown in Fig. 9, there was a statistically significant positive relationship between V_{max} and K_S values in the combined data from the Ross and Amundsen seas (r = 0.32, p < 0.5, n = 41), suggesting a biochemical trade-off between high affinity and high velocity C fixation. Such a trade-off has been previously observed for macronutrient uptake (see recent review by Litchman et al. 2007), but to our knowledge there are no comparable data for inorganic C, particularly for natural phytoplankton assemblages. A biochemical trade off between V_{max} and K_S is expected based on theoretical considerations of the Michealis–Menten equation for transport-mediated nutrient uptake systems. In this model, substrate (S) and transporter (T) react at a rate k_1 to produce a membrane complex (S–T), which delivers S into the cell (rate k_2) or releases S back into the extracellular environment (rate k_{-1}). By definition, K_S is derived as $(k_{-1} + k_2)/k_1$, while V_{max} is defined as $\sim k_2 \times$ [S–T] (Stryer 1988). In the case where the rate of nutrient release by the transporter back to environment is much lower than the rate of nutrient delivery to the cell, i.e. $k_{-1} \ll k_2$, K_S can be approximated as k_2/k_1. Both V_{max} and K_S are thus directly proportional to k_2, providing an explanation for the apparent coupling of high velocity (high V_{max}) and low affinity (high K_S) uptake.

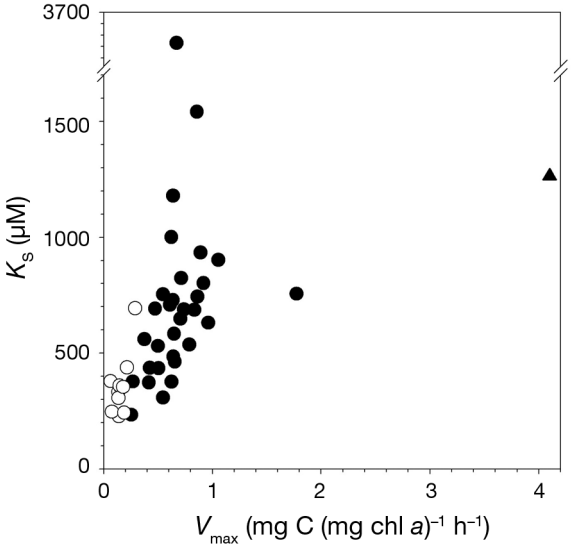

Fig. 9. Compilation of half-saturation constant (K_S) and biomass-normalized maximum C fixation rate (V_{max}) data for phytoplankton assemblages in the Ross Sea (open symbols) and Amundsen Sea (black symbols) polynas. The positive correlation between the variables is statistically significant at the 0.05 confidence level. A black triangle is used to denote one V_{max} value (stn 5 in the Amundsen Sea) where chl *a* concentrations may have been underestimated (see Table 1)

In addition to the differences in V_{max} and K_S described above, we observed differential CO_2-regulation of C fixation kinetics in the Amundsen and Ross seas. In the early season Ross Sea polynya, V_{max} showed a significant negative correlation with CO_2 (i.e. higher maximum fixation capacity under low CO_2 concentrations), whereas C uptake affinity (K_S) exhibited no apparent CO_2-dependent trend (Tortell et al. 2010). In contrast, our results from the Amundsen Sea show that CO_2 concentrations exerted a more significant effect on C uptake affinity (K_S) than V_{max} (Fig. 4). Part of this difference may reflect the different seasonal periods during which phytoplankton samples were collected in the Ross and Amundsen seas (October–November in the Ross Sea, and January–February in the Amundsen Sea). Macronutrients are plentiful in the early season Ross Sea polynya (following winter convection) and increased cellular RubisCO content may be a viable mechanism to increase V_{max} under low CO_2 conditions. In contrast, strong biological activity (fueled by enhanced Fe supply), combined with localized sea ice melt led to significant nutrient depletion in several regions of our Amundsen Sea survey. Under these potentially nutrient-limiting conditions, cells may down-regulate maximum C fixation capacity, and any CO_2 regulation of C uptake might occur primarily through changes in the substrate affinity of the C transport system (i.e. K_S).

C uptake in sea ice algae vs. phytoplankton

To date, only a few studies have examined the physiological mechanisms of C uptake in sea ice

algae, and all of this work has been conducted using mono-specific laboratory cultures. Mitchell & Beardall (1996) reported evidence for significant HCO_3^- transport, CA activity and intracellular CO_2 accumulation in the pennate ice diatom *Nitschia frigida*, indicative of CCM activity. In contrast, model calculations by Gleitz et al. (1996) suggested that diffusive CO_2 uptake was the dominant mode of C uptake in 3 of the 4 ice diatoms they examined. The laboratory data currently available thus suggest significant variability in C uptake across sea ice algal species, highlighting the importance of direct field observations of C uptake by diverse natural ice algal assemblages.

Field studies of sea ice algal physiology face a number of methodological challenges associated with spatial heterogeneity in the sea ice, and the need to isolate cells from a frozen matrix. Following the approach of previous authors (Arrigo et al. 2003a), we allowed ice samples to melt relatively slowly (up to 12 h) in a seawater dilution medium at ~0°C to minimize osmotic shock on algal populations. It is unclear whether these melting times would be sufficient to permit large shifts in cellular physiology as cells experience pCO_2 levels that may differ significantly from those in the sea ice. Mock & Valentin (2004) observed rapid (<12 h) changes in sea ice diatom photophysiology and RubisCO mRNA transcription in response to a large temperature shift, but no comparable data are available for rapid shifts in carbonate chemistry. Recent metagenomic analysis of sea ice algal assemblages from the Ross Sea (A. Allen pers. comm.) has demonstrated high *in situ* expression levels of genes encoding various CA isoforms and HCO_3^- transporters. These molecular data suggest that the high HCO_3^- uptake capacity and eCA expression observed in our physiological assays do indeed reflect the physiological potential of sea ice algae. We recognize, however, that the actual C fixation rates we measured may not provide an accurate reflection of *in situ* rates in the sea ice matrix where growth conditions (e.g. pH, pCO_2, and O_2 concentrations) may differ significantly from those in our standard assay conditions. A further complication concerns the quantification of relevant pCO_2 levels in sea ice samples. Our bulk CO_2 measurements in melted sea ice do not account for any spatial heterogeneity within the ice matrix, where potentially lower pCO_2 and higher chl *a* may occur in ice brine pockets (Thomas & Dieckmann 2002). Notwithstanding these caveats, our results should provide comparative insight into the C uptake potential in sea ice algae and phytoplankton.

The results shown in Table 4 demonstrate a wide range of C uptake affinities in the sea ice algal assemblages we sampled, relative to a more constrained range in the surface water Amundsen Sea phytoplankton assemblages (Table 2). The lowest C half-saturation constant we measured in sea ice (~100 µM DIC; Stn 33) was more than 2-fold lower than any values observed in Amundsen Sea surface waters, indicating a high capacity for photosynthesis under DIC-deplete conditions. In contrast, we also observed very low C uptake affinity (i.e. K_S > 4000 µM DIC) in some sea ice algae, even under conditions of severe CO_2 depletion (low bulk CO_2 concentrations). This result probably reflects growth limitation by low macronutrient concentrations (<1 µM NO_3^-) in many ice samples. Comparison of biomass-normalized V_{max} data from pelagic phytoplankton and sea ice algae (Fig. 6b), and results from photosynthesis–irradiance experiments (M. Mills unpubl.) show lower specific C turnover rates and light-saturated C fixation in the sea ice algal assemblages relative to phytoplankton assemblages (Alderkamp et al. 2012). Reduced C turnover rates in the sea ice algal assemblages could decrease cellular demands for CO_2 to the point where passive diffusion might be sufficient to sustain photosynthetic requirements, leading to a down regulation of the CCM. Slow growth rates would also explain the low relative eCA activity we observed in the sea ice algal assemblages relative to the phytoplankton assemblages (Fig. 6d). Our results thus underscore the potential importance of both inorganic supply and photosynthetic C demand as primary influences on the pathways of algal C acquisition (Rost et al. 2006).

C uptake and stable isotope fractionation

Rau et al. (1989) demonstrated a strong linear dependence of δ^{13}C-POC on surface water pCO_2 in Southern Ocean waters, and similar observations have been reported from laboratory phytoplankton culture experiments (Laws et al. 1995). These results led to the suggestion that sedimentary δ^{13}C values could be used as a paleo-proxy for ancient ocean pCO_2 levels. It is now apparent, however, that HCO_3^- transport and CCM activity can exert a strong influence on C isotope fractionation, leading to a decoupling of pCO_2 and δ^{13}C (Fielding et al. 1998, Keller & Morel 1999, Laws et al. 2002). In our data set, there was no apparent correlation between δ^{13}C-POC and CO_2 in surface water phytoplankton assemblages in the Amundsen Sea. We did, however, observe a sta-

tistically significant relationship between δ^{13}C-POC and a proxy variable for phytoplankton C demand: supply ratios (μ'; d^{-1}). This relationship underscores the influence of cellular C turnover rates on stable isotope fractionation, but the scatter in Fig. 7 indicates that other factors must also be considered. Laboratory data suggest that C isotope fractionation varies according to the nature of the growth-limiting resource, with a particular contrast between nutrient and light-dependent C fixation (Riebesell et al. 2000, Cassar et al. 2006). These differences probably reflect the unique constraints imposed by nutrient limitation (e.g. N constraints on RubisCO activity) and light limitation (restricted energy supplies to support the CCM). In the Amundsen Sea, both light and nutrient availability may constrain phytoplankton C fixation depending on mixed layer stratification and the extent of nutrient utilization in surface waters (Alderkamp et al. 2012). Unfortunately, none of the C uptake parameters we measured ($f_{HCO_3^-}$, V_{max}, K_S, eCA) showed any significant predictive power for δ^{13}C in a multiple regression analysis. Without more information, we are thus unable to provide a mechanistic explanation for the apparent variability in surface water δ^{13}C-POC in the Amundsen Sea.

By comparison with water-column measurements, relatively few measurements of δ^{13}C have been reported for sea-ice derived organic carbon. High sea ice δ^{13}C (i.e.^{13}C enrichment) has been taken as evidence for biological C depletion with limited C resupply from the external seawater environment (Kennedy et al. 2002, Papadimitriou et al. 2009, Munro et al. 2010). In addition, the intrinsic photosynthetic fractionation factor of the sea ice algae may decrease over time as the CO_2 supply becomes restricted and CCM activity is enhanced (Gleitz et al. 1995, Kennedy et al. 2002). Our δ^{13}C-POC sea ice data (range −12.85 to −25.65‰) are consistent with previous observations of high ^{13}C enrichment in ice-derived biogenic material. In the absence of δ^{13}C-DIC data, we cannot compute intrinsic photosynthetic fractionation factors. Our data do show, however, that the isotopic composition of the sea ice algae was not related to any of the physiological C uptake parameters we measured. Moreover, we observed no relationship between δ^{13}C and the apparent C demand/supply ratio in sea ice. This result may reflect, in part, the use of bulk melt CO_2 measurements, and the varying influences of both light and nutrient limitation on C fixation in the sea ice algae. A further complication is the potential for periodic exchange of DIC and POC with the surrounding seawater. This periodic exchange would act to partially reset any δ^{13}C signatures within the semi-enclosed sea ice matrix. We are thus unable, at present, to draw any firm conclusions on the relative importance of different factors controlling the isotopic composition of sea ice algal assemblages.

Conclusions and future outlook

Our results demonstrate high CCM capacity in Amundsen Sea phytoplankton assemblages, based on direct HCO_3^- transport coupled with moderate eCA activity. K_S for inorganic carbon in the Amundsen Sea phytoplankton were typically well below current surface water concentrations, suggesting that phytoplankton are currently DIC saturated and would thus show a limited response to future pCO_2 increases. Culture studies with Antarctic phytoplankton have shown mixed results with respect to CO_2-dependent responses. Riebesell et al. (1993) observed strong stimulation of Antarctic diatom growth under increased CO_2, while Boelen et al. (2011) observed no CO_2-dependent effects. Recent incubation experiments in the Ross Sea have demonstrated a small, though statistically significant, CO_2 stimulation of Fe-replete phytoplankton, with increasing diatom growth rates and primary production under high CO_2 conditions (Tortell et al. 2008, Feng et al. 2010). This CO_2-dependent productivity may reflect the down regulation of CCM activity and the corresponding re-allocation of energy to other metabolic processes (Hopkinson et al. 2011). In these experiments, large CO_2-dependent shifts in phytoplankton species assemblage composition were also observed, suggesting differential effects on various taxonomic groups. Although comparable incubation experiments have not been conducted in the Amundsen Sea, a similar response may be observed in this system given its similarity to the Ross Sea in terms of phytoplankton species assemblage composition and C uptake parameters (Fig. 8).

Predicting the response of sea ice algae to future environmental changes is more complicated than for open-water phytoplankton assemblages. A principal challenge is in understanding how future changes in mixed-layer chemistry may influence the internal dynamics of the semi-enclosed sea ice matrix. *In situ* biological and chemical processes appear to exert a first-order control on the carbonate chemistry of sea ice, with large variability resulting from autotrophic and heterotrophic processes and thermodynamic reactions within the carbonate system (Fransson et

al. 2011). While periodic exchange with ambient seawater may play a role in replenishing nutrients to sea ice algae near the ice/water interface, it is clear that the carbonate system in near-bottom ice can deviate significantly from that in the underlying water column. Our results suggest that sea ice algae exhibit high plasticity in terms of C uptake (e.g. large range in K_S; Table 4, Fig. 6c), so that the relatively small changes in background seawater DIC concentrations and speciation may not exert a significant influence on sea ice production.

Acknowledgements. This work was supported by research grants from NSERC (to P.D.T. and M.T.M.) and the National Science Foundation (DynaLiFe program, ANT-0732535 to A.A. and K.R.A.) as part of the International Polar Year. We thank Z. Brown (Stanford University) for field assistance with sea ice sampling and processing, K. Currie (NIWA) for assistance with DIC and alkalinity analysis and the crew and scientific personal of the ice breakers IB '*Nathanial B. Palmer*' and IB '*Oden*'.

LITERATURE CITED

Alderkamp AC, Mills MM, van Dijken GL, Laan P and others (2012) Iron from melting glaciers fuels phytoplankton blooms in the Amundsen Sea (Southern Ocean): phytoplankton characteristics and productivity. Deep-Sea Res II 71–76:32–48

Arrigo KR, Alderkamp AC (2012) Shedding dynamic light on Fe limitation (DynaLiFe) Introduction. Deep-Sea Res II 71–76:1–4

Arrigo KR, van Dijken GL (2003) Phytoplankton dynamics within 37 Antarctic coastal polynya systems. J Geophys Res C 108, 3271

Arrigo KR, Worthen D, Schnell A, Lizotte MP (1998) Primary production in Southern Ocean waters. J Geophys Res 103(C8):15587–15600

Arrigo KR, DiTullio GR, Dunbar RB, Robinson DH, VanWoert M, Worthen DL, Lizotte MP (2000) Phytoplankton taxonomic variability in nutrient utilization and primary production in the Ross Sea. J Geophys Res 105(C4): 8827–8846

Arrigo KR, Robinson DH, Dunbar RB, Leventer AR, Lizotte MP (2003a) Physical control of chlorophyll *a*, POC, and TPN distributions in the pack ice of the Ross Sea, Antarctica. J Geophys Res 108, 3316, doi:10.1029/2001JC001138

Arrigo KR, Worthen DL, Robinson DH (2003b) A coupled ocean-ecosystem model of the Ross Sea. 2. Iron regulation of phytoplankton taxonomic variability and primary production. J Geophys Res 108, 3231, doi:10.1029/2001JC000856

Arrigo KR, van Dijken G, Long M (2008) Coastal Southern Ocean: a strong anthropogenic CO_2 sink. Geophys Res Lett 35, L21602, doi:10.1029/2008GL035624

Arrigo KR, Lowry K, van Dijken G (2012) Annual changes in sea ice and phytoplankton in polynyas of the Amundsen Sea, Antarctica. Deep-Sea Res II 71–76:5–15

Badger MR, Price GD (1994) The role of carbonic anhydrase in photosynthesis. Annu Rev Plant Physiol Plant Mol Biol 45:369–392

Badger MR, Andrews TJ, Whitney SM, Ludwig M, Yellowlees DC, Leggat W, Price GD (1998) The diversity and coevolution of Rubisco, plastids, pyrenoids, and chloroplast-based CO_2-concentrating mechanisms in algae. Can J Bot 76:1052–1071

Bates NR, Hansell DA, Carlson CA, Gordon LI (1998) Distribution of CO_2 species, estimates of net community production, and air-sea CO_2 exchange in the Ross Sea polynya. J Geophys Res 103(C2):2883–2896

Boelen P, de Poll WHV, van der Strate HJ, Neven IA, Beardall J, Buma AGJ (2011) Neither elevated nor reduced CO_2 affects the photophysiological performance of the marine Antarctic diatom *Chaetoceros brevis*. J Exp Mar Biol Ecol 406:38–45

Cassar N, Laws EA, Bidigare RR, Popp BN (2004) Bicarbonate uptake by Southern Ocean phytoplankton. Global Biogeochem Cycles 18, GB2003, doi:10.1029/2003GB002116

Cassar N, Laws EA, Popp BN (2006) Carbon isotopic fractionation by the marine diatom *Phaeodactylum tricornutum* under nutrient-and light-limited growth conditions. Geochim Cosmochim Acta 70:5323–5335

Cavalieri D, Gloerson P, Zwally J (1990, updated 2006). DMSP SSM/I daily polar gridded sea ice concentrations. Maslanik J, Stroeve J (eds) National Snow and Ice Data Center, Boulder, CO. Digital media

Chierici M, Fransson A, Anderson LG (1999) Influence of m-cresol purple indicator additions on the pH of seawater samples: correction factors evaluated from a chemical speciation model. Mar Chem 65:281–290

Clayton TD, Byrne RH (1993) Spectrophotometric seawater pH measurements: total hydrogen ion concentration scale calibration of m-cresol purple and at-sea results. Deep-Sea Res I 40:2115–2129

Coale KH, Wang XJ, Tanner SJ, Johnson KS (2003) Phytoplankton growth and biological response to iron and zinc addition in the Ross Sea and Antarctic Circumpolar Current along 170 degrees W. Deep-Sea Res II 50:635–653

Delille B, Jourdain B, Borges AV, Tison JL, Delille D (2007) Biogas (CO_2, O_2, dimethylsulfide) dynamics in spring Antarctic fast ice. Limnol Oceanogr 52:1367–1379

Dickson AG (1990) Standard potential of the reaction: $AgCl(s) + 1/2H_2(g) = Ag(s) + HCl(aq)$, and and the standard acidity constant of the ion HSO_4^- in synthetic sea water from 273.15 to 318.15 K. J Chem Thermodyn 22: 113–127

DiTullio GR, Smith WO (1996) Spatial patterns in phytoplankton biomass and pigment distributions in the Ross Sea. J Geophys Res 101(C8):18467–18477

Elzenga JTM, Prins HBA, Stefels J (2000) The role of extracellular carbonic anhydrase activity in inorganic carbon utilization of *Phaeocystis globosa* (Prymnesiophyceae): a comparison with other marine algae using the isotopic disequilibrium technique. Limnol Oceanogr 45:372–380

Erez J, Bouevitch A, Kaplan A (1998) Carbon isotope fractionation by photosynthetic aquatic microorganisms: experiments with *Synechococcus* PCC7942, and a simple carbon flux model. Can J Bot 76:1109–1118

Espie GS, Colman B (1986) Inorganic carbon uptake during photosynthesis: 1: a theoretical anlaysis using the isotope disequilibrium technique. Plant Physiol 80:863–869

Feng Y, Hare CE, Rose JM, Handy SM and others (2010) Interactive effects of iron, irradiance and CO_2 on Ross Sea phytoplankton. Deep-Sea Res I 57:368–383

Fielding AS, Turpin DH, Guy RD, Calvert SE, Crawford DW, Harrison PJ (1998) Influence of the carbon concentrating mechanism on carbon stable isotope discrimination by the marine diatom *Thalassiosira pseudonana*. Can J Bot 76:1098–1103

Fransson A, Chierici M, Yager PL, Smith WO Jr (2011) Antarctic sea ice carbon dioxide system and controls. J Geophys Res 116, C12035, doi:10.1029/2010JC006844

Fujiki T, Matsumoto K, Honda MC, Kawakami H, Watanabe S (2009) Phytoplankton composition in the subarctic North Pacific during autumn 2005. J Plankton Res 31: 179–191

Gerringa LJA, Alderkamp AC, Laan P, Thuróczy CE and others (2012) Iron from melting glaciers fuels the phytoplankton blooms in Amundsen Sea (Southern Ocean): iron biogeochemistry. Deep-Sea Res II 71–76:16–31

Gibson JAE, Trull T, Nichols PD, Summons RE, McMinn A (1999) Sedimentation of ^{13}C-rich organic matter from Antarctic sea-ice algae: a potential indicator of past sea-ice extent. Geology 27:331–334

Giordano M, Beardall J, Raven JA (2005) CO_2 concentrating mechanisms in algae: mechanisms, environmental modulation, and evolution. Annu Rev Plant Biol 56: 99–131

Gleitz M, Thomas DN, Dieckmann GS, Millero FJ (1995) Comparison of summer and winter inorganic carbon, oxygen and nutrient concentrations in Antarctic sea ice brine. Mar Chem 51:81–91

Gleitz M, Kukert H, Riebesell U, Dieckmann GS (1996) Carbon acquisition and growth of Antarctic sea ice diatoms in closed bottle incubations. Mar Ecol Prog Ser 135: 169–177

Grasshoff K, Kremling K, Ehrhardt M (eds) (1999) Methods of seawater analysis. Wiley-VCH, Weinheim

Haraldsson C, Anderson LG, Hassellöv M, Hulth S, Olsson K (1997) Rapid, high-precision potentiometric titration of alkalinity in ocean and sediment pore waters. Deep-Sea Res I 44:2031–2044

Havskum H, Schlüter L, Scharek R, Berdalet E, Jacquet S (2004) Routine quantification of phytoplankton groups — microscopy or pigment analyses? Mar Ecol Prog Ser 273: 31–42

Holm-Hansen O, Lorenzen CJ, Holmes RW, Strickland JDH (1965) Fluorometric determination of chlorophyll. Rapp Cons Int Explor Mer 30:3–15

Hopkinson BM, Dupont CL, Allen AE, Morel FMM (2011) Efficiency of the CO_2-concentrating mechanism of diatoms. PNAS 108:3830–3837

Jacobs SS, Jenkins A, Giulivi CF, Dutrieux P (2011) Stronger ocean circulation and increased melting under Pine Island Glacier ice shelf. Nat Geosci 4:519–523

Kattner G, Thomas DN, Haas C, Kennedy H, Dieckmann GS (2004) Surface ice and gap layers in Antarctic sea ice: highly productive habitats. Mar Ecol Prog Ser 277:1–12

Keller K, Morel FMM (1999) A model of carbon isotopic fractionation and active carbon uptake in phytoplankton. Mar Ecol Prog Ser 182:295–298

Kennedy H, Thomas DN, Kattner G, Haas C, Dieckmann GS (2002) Particulate organic matter in Antarctic summer sea ice: concentration and stable isotopic composition. Mar Ecol Prog Ser 238:1–13

Kozlowski WA, Deutschman D, Garibotti I, Trees C, Vernet M (2011) An evaluation of the application of CHEMTAX to Antarctic coastal pigment data. Deep-Sea Res I 58: 350–364

Laws EA, Popp BN, Bidigare RR, Kennicutt MC, Macko SA (1995) Dependence of phytoplankton carbon isotopic composition on growth rate and $[CO_2]_{aq}$: theoretical considerations and experimental results. Geochim Cosmochim Acta 59:1131–1138

Laws EA, Popp BN, Cassar N, Tanimoto J (2002) ^{13}C discrimination patterns in oceanic phytoplankton: likely influence of CO_2 concentrating mechanisms, and implications for palaeoreconstructions. Funct Plant Biol 29:323–333

Litchman E, Klausmeier CA, Schofield OM, Falkowski PG (2007) The role of functional traits and trade-offs in structuring phytoplankton communities: scaling from cellular to ecosystem level. Ecol Lett 10:1170–1181

Mackey MD, Mackey DJ, Higgins HW, Wright SW (1996) CHEMTAX — a program for estimating class abundances from chemical markers: application to HPLC measurements of phytoplankton. Mar Ecol Prog Ser 144: 265–283

Mackey DJ, Higgins HW, Mackey MD, Holdsworth D (1998) Algal class abundances in the western equatorial Pacific: estimation from HPLC measurements of chloroplast pigments using CHEMTAX. Deep-Sea Res I 45:1441–1468

Martin CL, Tortell PD (2006) Bicarbonate transport and extracellular carbonic anhydrase activity in Bering Sea phytoplankton assemblages: results from isotope disequilibrium experiments. Limnol Oceanogr 51: 2111–2121

Meiners KM, Papadimitriou S, Thomas DN, Norman L, Dieckmann GS (2009) Biogeochemical conditions and ice algal photosynthetic parameters in Weddell Sea ice during early spring. Polar Biol 32:1055–1065

Miki M, Ramaiah N, Takeda S, Furuya K (2008) Phytoplankton dynamics associated with the monsoon in the Sulu Sea as revealed by pigment signature. J Oceanogr 64: 663–673

Mitchell C, Beardall J (1996) Inorganic carbon uptake by an Antarctic sea-ice diatom, *Nitzschia frigida*. Polar Biol 16: 95–99

Mock T, Valentin K (2004) Photosynthesis and cold acclimation: molecular evidence from a polar diatom. J Phycol 40:732–741

Mook WG, Bommerson JC, Staverman WH (1974) Carbon isotope fractionation between dissolved bicarbonate and gaseous carbon dioxide. Earth Planet Sci Lett 22:169–176

Munro DR, Dunbar RB, Mucciarone DA, Arrigo KR, Long MC (2010) Stable isotope composition of dissolved inorganic carbon and particulate organic carbon in sea ice from the Ross Sea, Antarctica. J Geophys Res 115, C09005, doi:10.1029/2009JC005661

Neven IA, Stefels J, van Heuven SMAC, de Baar HJW, Elzenga JTM (2011) High plasticity in inorganic carbon uptake by Southern Ocean phytoplankton in response to ambient CO_2. Deep-Sea Res II 58:2636–2646

Papadimitriou S, Thomas DN, Kennedy H, Kuosa H, Dieckmann GS (2009) Inorganic carbon removal and isotopic enrichment in Antarctic sea ice gap layers during early austral summer. Mar Ecol Prog Ser 386:15–27

Pierrot D, Lewis E, Wallace DWR (2006) MS Excel program developed for CO_2 system calculations. ORNL/CDIAC-105, Carbon Dioxide Information Analysis Center, Oak Ridge National Laboratory, US Department of Energy, Oak Ridge, TN

Rau GH, Takahashi T, Marais DJD (1989) Latitudinal variations in plankton δ^{13}C: implications for CO_2 and productivity in past oceans. Nature 341:516–518

Riebesell U (2004) Effects of CO_2 enrichment on marine phytoplankton. J Oceanogr 60:719–729

Riebesell U, Wolfgladrow DA, Smetacek V (1993) Carbon dioxide limitation of marine phytoplankton growth rates. Nature 361:249–251

Riebesell U, Burkhardt S, Dauelsberg A, Kroon B (2000) Carbon isotope fractionation by a marine diatom: dependence on the growth-rate-limiting resource. Mar Ecol Prog Ser 193:295–303

Rodriguez F, Varela M, Zapata M (2002) Phytoplankton assemblages in the Gerlache and Bransfield straits (Antarctic Peninsula) determined by light microscopy and CHEMTAX analysis of HPLC pigment data. Deep-Sea Res II 49:723–747

Rost B, Riebesell U, Burkhardt S, Sultemeyer D (2003) Carbon acquisition of bloom-forming marine phytoplankton. Limnol Oceanogr 48:55–67

Rost B, Riebesell U, Sultemeyer D (2006) Carbon acquisition of marine phytoplankton: effect of photoperiod length. Limnol Oceanogr 51:12–20

Roy RN, Roy LN, Vogel KM, Porter-Moore C and others (1993) The dissociation constants of carbonic acid in seawater at salinities 5 to 45 and temperatures 0 to 45°C. Mar Chem 44:249–267

Sedwick PN, DiTullio GR (1997) Regulation of algal blooms in Antarctic shelf waters by the release of iron from melting sea ice. Geophys Res Lett 24:2515–2518

Silverman DN (1982) Carbonic anhydrase: oxygen-18 exchange catalzyed by an enzyme with rate-contributing proton transfer steps. Methods Enzymol 87:732–752

Smith WO, Nelson DM (1985) Phytoplankton bloom produced by a receding ice edge in the Ross Sea — spatial coherence with the density field. Science 227:163–166

Smith WO, Marra J, Hiscock MR, Barber RT (2000) The seasonal cycle of phytoplankton biomass and primary productivity in the Ross Sea, Antarctica. Deep-Sea Res II 47: 3119–3140

Stoecker DK, Gustafson DE, Baier CT, Black MMD (2000) Primary production in the upper sea ice. Aquat Microb Ecol 21:275–287

Stryer L (1988) Biochemistry. 3rd Edn. WH Freeman, New York, NY

Suzuki K, Minami C, Liu H, Saino T (2002) Temporal and spatial patterns of chemotaxonomic algal pigments in the subarctic Pacific and the Bering Sea during the early summer of 1999. Deep-Sea Res II 49:5685–5704

Sweeney C, Hansell DA, Carlson CA, Codispoti LA and others (2000) Biogeochemical regimes, net community production and carbon export in the Ross Sea, Antarctica. Deep-Sea Res II 47:3369–3394

Thomas DN, Dieckmann GS (2002) Antarctic sea ice — a habitat for extremophiles. Science 295:641–644

Tortell PD, Morel FMM (2002) Sources of inorganic carbon for phytoplankton in the eastern subtropical and equatorial Pacific Ocean. Limnol Oceanogr 47:1012–1022

Tortell PD, Martin CL, Corkum ME (2006) Inorganic carbon uptake and intracellular assimilation by subarctic Pacific phytoplankton assemblages. Limnol Oceanogr 51: 2102–2110

Tortell PD, Payne CD, Li YY, Trimborn S and others (2008) CO_2 sensitivity of Southern Ocean phytoplankton. Geophys Res Lett 35, L04605, doi:10.1029/2007GL032583

Tortell PD, Trimborn S, Li Y, Rost B, Payne CD (2010) Inorganic carbon utilization by Ross Sea phytoplankton across natural and experimental CO_2 gradients. J Phycol 46:433–443

Tortell PD, Guéguen C, Long MC, Payne CD, Lee P, DiTullio GR (2011) Spatial variability and temporal dynamics of surface water pCO_2, $\Delta O_2/Ar$ and dimethylsulfide in the Ross Sea, Antarctica. Deep-Sea Res I 58:241–259

Tortell PD, Long MC, Payne CD, Alderkamp AC, Dutrieux P, Arrigo KR (2012) Spatial distribution of pCO_2, $\Delta O_2/Ar$ and dimethylsulfide (DMS) in polynya waters and the sea ice zone of the Amundsen Sea, Antarctica. Deep-Sea Res II 71–76:77–93

Vidussi F, Roy S, Lovejoy C, Gammelgaard M and others (2004) Spatial and temporal variability of the phytoplankton community structure in the North Water polynya, investigated using pigment biomarkers. Can J Fish Aquat Sci 61:2038–2052

Villinski JC, Dunbar RB, Mucciarone DA (2000) Carbon 13/Carbon 12 ratios of sedimentary organic matter from the Ross Sea, Antarctica: a record of phytoplankton bloom dynamics. J Geophys Res 105(C6):14163–14172

Walker DP, Brandon MA, Jenkins A, Allen JT, Dowdeswell JA, Evans J (2007) Oceanic heat transport onto the Amundsen Sea shelf through a submarine glacial trough. Geophys Res Lett 34, L02602, doi:10.1029/2006GL 028154

Wright SW, Thomas DP, Marchant HJ, Higgins HW, Mackey MD, Mackey DJ (1996) Analysis of phytoplankton of the Australian sector of the Southern Ocean: comparisons of microscopy and size frequency data with interpretations of pigment HPLC data using the 'CHEMTAX' matrix factorisation program. Mar Ecol Prog Ser 144: 285–298

Zapata M, Rodriguez F, Garrido JL (2000) Separation of chlorophylls and carotenoids from marine phytoplankton: a new HPLC method using a reversed phase C_8 column and pyridine-containing mobile phases.

Editorial responsibility: Ronald Kiene, Mobile, Alabama, USA

Submitted: October 5, 2012; Accepted: January 22, 2013
Proofs received from author(s): April 29, 2013